DAGLβ Inhibition Perturbs a Lipid Network Involved in Macrophage Inflammatory Responses

Ku-Lung Hsu, Katsunori Tsuboi, Alexander Adibekian, Holly Pugh, Kim Masuda, and Benjamin F. Cravatt.

SUPPLEMENTARY INFORMATION

SUPPLEMENTARY METHODS

Materials. Pharmacological studies were conducted in C57Bl/6 mice unless indicated otherwise. *Pla2g4a*$^{+/+}$ and *Pla2g4a*$^{-/-}$ mice on a BALB/c background were generated as previously described[1] and obtained from Joseph Bonventre's laboratory at Brigham and Women's Hospital. In brief, gene-targeting in mouse embryonic stem (ES) cells was used to disrupt an exon (amino acids 187-232, NM_008869.3) in the PLA2G4A gene. Mice generated from targeted clones were genotyped by Southern blotting and the absence of PLA2G4A protein in *Pla2g4a*$^{-/-}$ mice was confirmed by western blotting. FP-rhodamine and FP-biotin were synthesized according to a previously described protocol[2]. All triazole-urea compounds were synthesized in the laboratory. In general, the triazole-urea compounds reported in these studies were soluble in DMSO at concentrations of 10-50 mM for use in cellular and *in vitro* studies. For *in vivo* studies in mice, KT172, KT109, and KT195 were solubilized in an 18:1:1 solution of saline:emulphor:ethanol and sonicated for ~ 5 min before administration to mice. We found that KT172 showed the best solubility in 18:1:1 vehicle and dissolved almost completely in solution. KT109 and KT195 both produced a uniform suspension in 18:1:1 vehicle. We found that all three compounds could be administered to rodents by intraperitoneal (i.p.) injection to efficiently inactivate their target enzymes. All other chemicals and reagents were purchased from Sigma. All deuterated lipid standards and substrates were purchased from Cayman Chemicals. The Mouse Inflammatory Cytokines Single-Analyte ELISArray kit was purchased from Qiagen. Neuro2A and HEK293T cells were obtained from ATCC. Full-length cDNAs encoding serine hydrolases were purchased from Open Biosystems.

Generation of DAGL knockout mice. *Daglb*$^{+/+}$, *Daglb*$^{+/-}$, and *Daglb*$^{-/-}$ mice were on a mixed genetic background of C57Bl/6 and 129/SvEv and were obtained from Taconic. In brief, *Daglb*$^{-/-}$ mice were generated from a Lexicon OmniBank ES cell clone OST195261 that contains a gene trap cassette insertion in the first exon of DAGLβ (NM_144915.2). *Daglb* genotypes were determined by PCR amplification of genomic tail DNA using the following primers designed by Taconic: *Daglb* forward 5′ - AAGGAGGCAAAGACAGCAAAGTGC-3′ , *Daglb* reverse 5′ - TATCCTAGGTGCAGACAGATTGTGC-3′ , and gene trap forward 5′ - AAATGGCGTTACTTAAGCTAGCTTGC-3′ , which amplified a 390-bp product for the wild-type allele and a 195-bp product for the gene-trapped allele.

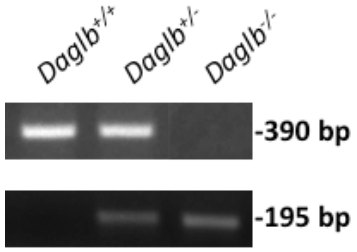

Representative agarose gel of *Daglb* mice genotypes determined by PCR amplification of genomic tail DNA.

Dagla$^{-/-}$ mice were generated as previously described[3] using a targeting vector that deleted exon 1 and contained 4 and 9.5 kb of mouse genomic DNA 5' and 3' of DAGLα (NC_000011.8) exon 1, respectively using the RedET recombineering system (Gene Bridges) following the manufacturer's protocol. In collaboration with The Scripps Research Institute Murine Genetics Core, the construct (kind gift from Pfizer) was electroporated into C57Bl/6 embryonic stem (ES) cells and homologously targeted clones were selected and identified using standard procedures. Mouse lines were

derived from targeted clones using standard procedures and maintained on a C57Bl/6 background. *Dagla* genotypes were identified by Southern blotting of genomic tail DNA using probes external to the targeting vector that were derived by PCR from mouse genomic DNA using the following primers: 5' external probe; 5'-GAGCTCTGTTCAGGTGGTTCG; 5'-CTGGGCACCTTCTTTGATCC; 3' external probe; 5'-GGAAATCACAGCTGGTAGCC; 5'- CTGCTCTTCAGGAACTCAGG. Both probes detect an endogenous band of 16.4 kb in NdeI-digested genomic DNA from *Dagla*$^{+/+}$ mice and bands of 8.6 and 11.1 kb in *Dagla*$^{-/-}$ mice using the 5' or 3' external probes, respectively. The absence of DAGLα protein in *Dagla*$^{-/-}$ mice was confirmed by western blotting (**Supplementary Fig. 21b**) using an anti-mouse DAGLα polyclonal antibody raised in rabbit (kind gift from Professor Masahiko Watanabe) and gel-based ABPP using HT-01 (**Supplementary Fig. 21a**).

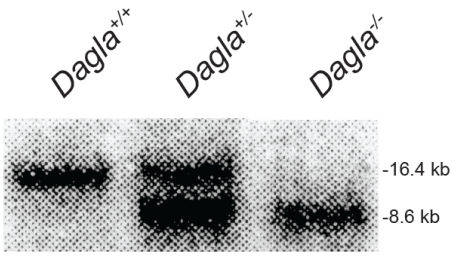

Representative blot of *Dagla* mice genotypes determined by Southern blotting of NdeI-digested genomic tail DNA (5' external probe is shown).

M**etabolite measurements.** All of our lipidomic analyses were performed in serum-free media to minimize the contribution of serum lipids to our studies. Metabolites were quantified by either selected reaction monitoring (SRM) of each metabolite using an Agilent G6410B Triple-Quad instrument or untargeted metabolomic analysis (substrate assays) using an Agilent 1100 series LC-MSD SL instrument. Liquid chromatography (LC) separation was achieved with a Gemini reverse-phase C18 column (50 mm, 4.6

mm with 5 μm diameter particles, Phenomonex) together with a pre-column (C18, 3.5 μm, 2 mm x 20 mm). For analysis of diacylglycerols (DAGs) a Luna C5 column (50 mm x 4.60 mm with 5 μm diameter particles) from Phenomenex was used. Mobile phase A was made of 95:5 v/v H_2O:MeOH, and mobile phase B was composed of 60:35:5 v/v/v i-PrOH:MeOH:H_2O. Ammonium hydroxide (0.1%) and formic acid (0.1%) was included to assist in ion formation in negative and positive ionization modes, respectively. For analysis of DAGs, 5 mM ammonium formate was also used in addition to 0.1% formic acid to assist in positive ionization and NH_4+ adduct formation. For metabolite measurements, cells were resuspended in 1 mL of a 1% NaCl solution and added to 3 mL of a 2:1 v/v $CHCl_3$:MeOH doped with 1 nmol of the following internal standards: d_5-2-arachidonoylglycerol (2-AG), d_8-arachidonic acid (AA), and d_8-1-stearoyl-2-arachidonoylglycerol (SAG), d_4-leukotriene B4 (LTB4), d_9-prostaglandin E2 (PGE2), d_9-prostaglandin D2 (PGD2) and d_8-anandamide (AEA), and d_4-8-*iso*-$PGF_{2\alpha}$. The mixture was vortexed and then centrifuged (1,400 x *g*, 3 min). The organic layer was removed, $CHCl_3$ was added until the final volume was again 4 ml, and the extraction was repeated. The combined organic extracts were dried under a stream of N_2 and resolubilized in 2:1 v/v $CHCl_3$:MeOH (120 μl). 30 μL of resolubilized lipids were injected for positive mode (MAGs and DAGs) and negative mode (free fatty acids and eicosanoids) measurements.

For targeted analysis in positive mode, the flow rate for each run started at 0.1 mL/min with 0% B. At 5 min, the solvent was changed immediately to 60% B with a flow rate of 0.4 mL/min and increased linearly to 100% B over 15 min. This was followed by an isocratic gradient of 100% B for 8 min at 0.5 mL/min before equilibrating for 3 min at 0% B at 0.5 mL/min. For targeted analysis in negative mode, the flow rate for each run started at 0.1 mL/min with 0% B. At 3 min, the flow rate was increased by 0.4 mL/min with a linear increase of solvent B to 100% over 17 min. This was followed by isocratic

gradient of 100% B for 7 min at 0.5 mL/min before equilibrating for 3 min with 0% B at 0.5 mL/min. For measurement of hydrolysis products in enzyme substrate assays (positive mode), the flow rate for each run started at 0.1 mL/min with 0% B. At 5 min, the solvent was changed immediately to 100% B with a flow rate of 0.4 mL/min. This was followed by an isocratic gradient of 100% B for 5 min at 0.5 mL/min before equilibrating for 5 min with 0% B at 0.5 mL/min.

The following parameters (MS) were used to measure the indicated metabolites by SRM (precursor ion, product ion, collision energy in V, polarity): C20:4 MAG or 2-AG (379, 287, 8, positive), d_5-2-AG (384, 287, 5, positive), C18:0/C20:4 DAG or SAG (662, 341, 15, positive), d_8-SAG (671, 671, 0, positive), C18:1/C20:4 DAG (660, 341, 15, positive), C16:0/C20:4 DAG (634, 341, 15, positive), C14:0/C20:4 DAG (606, 341, 15, positive), d_8-AEA (354.6, 63.2, 7, positive), AEA (348, 62, 11, positive), arachidonic acid or AA (303, 303, 0, negative), d_8-AA (311, 267, 5, negative), PGE2 (351, 271, 10, negative), PGD2 (351, 271, 10, negative), d_4-LTB4 (339.5, 196.9, 3, negative), d_9-PGE2 (360.5, 121.9, 25, negative), d_9-PGD2 (360.5, 281, 15, negative), TXB2 (369, 195, 5, negative), LTB4 (335, 195, 3, negative), d_4-8-*iso*-$PGF_{2\alpha}$ (357.5, 196.9, 15, negative), 8-*iso*-$PGF_{2\alpha}$ (353, 193, 15, negative), LTA4 (317, 163, 3, negative), LTC4 (624, 272, 3, negative), LTD4 (495, 177, 3, negative), and LTE4 (438, 333, 3, negative). MS analysis was performed with an electrospray ionization source with the following parameters: drying gas temperature = 350 ºC, drying gas flow rate = 11 L/min, and the nebulizer pressure = 35 psi. Prostaglandin SRM parameters were based on previously reported methods and transitions[4]. Metabolites targeted by SRM were quantified by measuring the area under the peak in comparison with the internal standards. Experiments were performed twice, and data sets were pooled for SAG, AA, PGE2, and PGD2 analyses in peritoneal macrophages from C57Bl/6 mice; a representative data set was shown for 2-AG. In DAGL substrate assays, formation of the hydrolysis product, 2-AG was followed

by measuring the area under the peak for 2-AG in comparison to the 1-monopentadecanoin standard ion. We also attempted to measure additional eicosanoids, including $PGF_{2\alpha}$, LTA_4, LTC_4, LTD_4, and LTE_4, but could not detect these lipids in macrophages using our targeted LC-MS methods.

Measurement of brain and liver lipids. Brain or liver tissue was weighed and subsequently Dounce homogenized in 2:1:1 v/v/v $CHCl_3$:MeOH:1% NaCl (8 ml) containing d_5-2-arachidonoylglycerol (2-AG) and d_8-arachidonic acid (AA). The mixture was vortexed and then centrifuged (1,400 x *g*, 3 min). The organic layer was removed, $CHCl_3$ was added until the final volume was again 8 ml, and the extraction was repeated. The combined organic extracts were dried under a stream of N2 and resolubilized in 2:1 v/v $CHCl_3$:MeOH (120 µl). 10 µL of resolubilized lipid were injected for positive mode (2-AG) and negative mode (AA) measurements, respectively. Lipid measurements were performed by LC-MS as described above.

DAGL hydrolysis assay. The activity of DAGL-alpha and -beta (DAGLα and DAGLβ) was determined using recombinant V5-tagged protein overexpressed in HEK293T cells as previously described[5] with some minor modifications. HEK293T-DAGLα or -DAGLβ membrane lysates were diluted to 2 mg/mL or 0.3 mg/mL (70 µL sample volume) respectively, in DAGL solution (5 mM $CaCl_2$, 100 mM NaCl, 50 mM HEPES). Lysates were treated with DMSO or compound for 30 min at 37 ºC. The substrate was prepared by sonicating 1-stearoyl-2-arachidonoylglycerol (SAG) in DAGL solution (5 mM $CaCl_2$, 100 mM NaCl, 50 mM HEPES) + 0.005% and 0.5% Triton X-100 for DAGLα and DAGLβ, respectively. The substrate was added to the sample reaction (30 µL, 500 µM final concentration of SAG), sonicated for 5 sec, and then incubated for 30 min at 37 ºC.

The reaction was quenched by adding 300 μL of 2:1 v/v $CHCl_3$:MeOH, doped with 1 nmol of 1-monopentadecanoin standard, vortexed and then centrifuged (1,400 x *g*, 3 min) to separate the phases. The organic phase was subjected to LC-MS analysis and 2-AG was quantified as described above.

Preparation of mouse tissue proteomes. Mouse brains or livers were Dounce-homogenized in PBS, pH 7.5, followed by a low-speed spin (1,400 x *g*, 5 min) to remove debris. The supernatant was then subjected to centrifugation (100,000 x *g*, 45 min) to yield the cytosolic fraction in the supernatant and the membrane fraction as a pellet. The pellet was washed and resuspended in PBS buffer by sonication. Total protein concentration in each fraction was determined using a protein assay kit (Bio-Rad). Samples were stored at -80°C until use.

Gel-based competitive ABPP. Gel-based competitive ABPP experiments were performed as previously described[6,7]. Proteomes (1 mg/mL) were treated with either FP-rhodamine or HT-01 (1 μM final concentration) in a 50 μL total reaction volume. After 30 min at 37 ºC, the reactions were quenched with SDS-PAGE loading buffer. After separation by SDS-PAGE (10% acrylamide), samples were visualized by in-gel fluorescence scanning using a flatbed fluorescent scanner (Hitachi FMBio IIe). To measure DAGLα activity, proteomes were diluted to 2 mg/mL and samples were not boiled prior to SDS-PAGE. Boiling appears to impair migration of DAGLα protein in gels and reduces signal intensity due to factors that we do not fully understand.

Assigning serine hydrolases to FP-rhodamine labeled bands on ABPP gels. We utilized a combination of approaches to confirm the identity of FP-rhodamine-labeled

protein bands on SDS-PAGE gels. These approaches extend beyond just correlations with predicted molecular weight to include: 1) confirmation of the absence of the protein band in knockout mice lacking the enzyme, and/or 2) confirmation of the absence of the protein band in proteomic samples treated with selective inhibitors of the enzyme. We also measured the loss of enzyme activities by mass spectrometry-based ABPP methods (see below), which added confidence to our gel-based assignments [e.g., in Neuro2A cells, the 70 kDa target of the HT-01 activity probe is blocked by KT109 and KT172, but not KT195 (**Fig. 2c**), and the ABPP-SILAC data show that the only serine hydrolase activity that matches this gel profile is DAGLβ, a 70 kDa enzyme (**Fig. 3c**)]. We also took advantage, where necessary, of profiling recombinantly expressed enzymes in transfected cell extracts[6]. This is important for serine hydrolases that are too low in abundance to evaluate in native cell or tissue proteomes by gel-based ABPP methods. The bands shown in **Figures 1-4** originate from either mouse cells/tissues (FAAH, MGLL, ABHD12, ABHD6, and LYPLA1/2) or transfected cell systems (DAGLβ, ABHD11, PLA2G7, and PAFAH2). For those enzymes profiled in mouse cells/tissues, we have confirmed their band identities in the current or past studies using knockout mice [DAGLβ (current study), FAAH[8], MGLL[9]] and/or selective inhibitors [DAGLβ (current study), FAAH[10]; MGLL[5], ABHD6[11], ABHD12[12], LYPLA1/2[13]]. For those enzymes profiled in transfected cell systems (DAGLβ, ABHD11, PLA2G7, PAFAH2), we confirmed their band identities by comparisons to mock-transfected cells (for DAGLβ, see **Supplementary Fig. 5**; for ABHD11, PAFAH2, and PLA2G7, see [6]).

ABPP-SILAC sample preparation and analysis. The soluble and membrane fractions were isolated by centrifugation (100K x *g*, 45 min) and the protein concentration for each fraction was adjusted to 2 mg/mL with DPBS. The light and heavy proteomes were

labeled with the activity-based affinity probe FP-biotin (500 μL total reaction volume, 10 μM final concentration) for 2 h at 25 ºC. After incubation, light and heavy proteomes were mixed in 1:1 ratio, and the membrane proteomes were additionally solubilized with 1% Triton-X100. Samples were desalted over PD10 columns (GE Healthcare) in DPBS, and biotinylated proteins enriched with streptavidin beads (50 μL beads; conditions: 1 h, 25 °C, 0.5% SDS in DPBS). The beads were washed with 1% SDS in DPBS (1x), 6 M urea (1x), and DPBS (2x), then resuspended in 6 M urea (150 μL), reduced with 5 mM TCEP for 20 min, and alkylated with 10 mM iodoacetamide for 30 min at 25 °C in the dark. The urea concentration was reduced to 2 M with 2x volume DPBS. On-bead digestions were performed for 12 h at 37 °C with sequence-grade modified trypsin (Promega; 2 μg) in the presence of 2 mM $CaCl_2$. Peptide samples were acidified to a final concentration of 5% (v/v) formic acid and stored at -80 °C prior to analysis. To distinguish non-specific proteins from proteins that react specifically with FP-biotin, we have previously performed extensive “probe” versus “no-probe” control experiments [6,7,14], where we compare the SILAC ratios or spectral counts of proteins from samples treated with or without the FP-biotin probe. In these experiments, only serine hydrolases that show greater than 5-fold increases in signals (SILAC ratios or spectral counts) in probe reactions compared to no-probe reactions are considered specific targets of the FP probe and analyzed further. Proteins that, on the other hand, exhibit near equal signals in probe- versus no-probe reactions are considered background proteins that bind to the avidin beads non-specifically and are removed from our analyses. In the current manuscript, we have restricted our analysis to serine hydrolases that have been established as specific targets of FP probes based on these past studies. See **Supplementary Dataset 1** for complete proteomic data and extracted serine hydrolase data.

ABPP-MudPIT sample preparation and analysis. Peritoneal macrophage proteomes were adjusted to a final protein concentration of 2 mg/mL and labeled with FP-biotin (500 μL total reaction volume, 10 μM final concentration) for 2 hours at 25 ºC. After incubation the proteomes were additionally solubilized with 1% Triton-X100. Samples were desalted over PD10 columns (GE Healthcare) in DPBS, and biotinylated proteins enriched with streptavidin beads (50 μL beads; conditions: 1 h, 25 °C, 0.5% SDS in DPBS). The beads were washed with 1% SDS in DPBS (1x), 6 M urea (1x), and DPBS (2x), then resuspended in in 6 M urea (150 μL), reduced with 5 mM TCEP for 20 minutes, and alkylated with 10 mM iodoacetamide for 30 minutes at 25 °C in the dark. The urea concentration was reduced to 2 M with 2x volume DPBS. On-bead digestions were performed for 12 h at 37 °C with sequence-grade modified trypsin (Promega; 2 μg) in the presence of 2 mM $CaCl_2$. Peptide samples were acidified to a final concentration of 5% (v/v) formic acid and stored at -80 °C prior to analysis. Serine hydrolase activities were extracted from complete proteomic data using the criteria described above to distinguish specific, FP-biotin-labeled proteins from background proteins. See **Supplementary Dataset 2** for complete proteomic data and extracted serine hydrolase data.

Determination of IC_{50} values. For gel-based competitive ABPP studies, proteomes from cells treated *in situ* with inhibitor for 4 h at 37 °C at the indicated concentrations (n = 3) were labeled with HT-01 (1 μM) for 30 min at 37 °C. After quenching, SDS-PAGE, and in-gel visualization, the percentage of enzyme activity remaining was determined by measuring the integrated optical intensity of the bands using ImageJ software. For LC-MS substrate assays, the percentage of enzyme activity remaining was determined by

comparing the specific activity (amount of 2-AG formed per min per mg of proteome) of inhibitor- with DMSO-treated samples. Nonlinear regression analysis was used to determine the IC_{50} values from a dose-response curve generated using GraphPad Prism

LC-MS/MS analysis of SILAC samples. Samples were analyzed by multidimensional liquid chromatography tandem mass spectrometry (MudPIT) using an Agilent 1200-series quaternary pump and Thermo Scientific LTQ-Orbitrap ion trap mass spectrometer as previously described. Peptides were eluted in a 5-step MudPIT experiment using 0%, 25%, 50%, 80%, and 100% salt bumps of 500 mM aqueous ammonium acetate and data were collected in data-dependent acquisition mode with dynamic exclusion turned on (20 s, repeat of 1). Specifically, one full MS (MS1) scan (400-1800 m/z) was followed by 30 MS2 scans of the most abundant ions. The MS2 spectra data were extracted from the raw file using RAW Xtractor (version 1.9.9.2; publicly available at http://fields.scripps.edu/downloads.php). MS2 spectra data were searched using the ProLuCID algorithm (publicly available at http://fields.scripps.edu/downloads.php) against the latest version of the mouse IPI database concatenated with the reversed database for assessment of false-discovery rates. ProLucid searches allowed for static modification of cysteine residues (+57.02146 due to alkylation), methionine oxidation (+15.9949), mass shifts of labeled amino acids (+10.0083 R, +8.0142 K) and no enzyme specificity. The resulting MS2 spectra matches were assembled into protein identifications and filtered using DTASelect (version 2.0) using the --modstat, --mass, and --trypstat options (applies different statistical models for the analysis of high resolution masses, peptide digestion state, and methionine oxidation state respectively). Ratios of heavy/light (test compound/DMSO) peaks were calculated using in-house software and normalized at the peptide level to the average ratio of all non-serine hydrolase peptides. Reported ratios represent the mean of all unique, quantified

peptides per protein and do not include peptides that were >3 standard deviations from the median peptide value. Proteins with less than two peptides per protein ID were not included in the analysis.

LC-MS/MS analysis of *in vivo* samples. Samples were digested and acidified peptide mixtures were analyzed by two-dimensional liquid chromatography/tandem mass spectrometry (MudPIT) using an Agilent 1200-series quaternary pump and Thermo Scientific LTQ ion trap mass spectrometer. Spectral counts were calculated for all serine hydrolases with an average of 4 or more spectral counts in the DMSO control samples except ABHD6, which was included even if signal intensities were below the cutoff. Spectral counts are reported as the average of three samples with the standard error of the mean (SEM).

Statistical analysis. Data are shown as mean $\pm$ s.e.m. Student's t test (unpaired, two-tailed) was used to determine differences between two groups. A p value of < 0.05 was considered significant. All statistical analyses were performed using GraphPad Prism.

General synthetic methods. All chemicals and reagents were purchased from Sigma-Aldrich, Acros, Fisher, Fluka, Maybridge, Combi-Blocks, BioBlocks, and Matrix Scientific and used without further purification unless noted otherwise. Dry solvents were obtained by passing commercially available pre-dried, oxygen-free formulations through activated alumina columns. All reactions were carried out under a nitrogen atmosphere using oven-dried glassware except where noted. Flash chromatography was carried out using 230-400 mesh silica gel. ^{1}H-NMR and ^{13}C-NMR spectra were recorded in $CDCl_3$ on a Varian Mercury-300 spectrometer, a Varian Inova-400 or a Bruker DRX-600 spectrometer, and were referenced to trimethylsilane (TMS). Chemical shifts were

reported in ppm relative to TMS and *J* values were reported in Hz. High resolution mass spectrometry (HRMS) experiments were performed at The Scripps Research Institute Mass Spectrometry Core on an Agilent mass spectrometer using electrospray ionization-time of flight (ESI-TOF). Crystal structures were solved at the University of California San Diego (UCSD) Small Molecule X-ray Crystallography Facility. The quality of all Crystallographic Information Files (CIF) was validated using the web-based checkCIF/PLATON service (http://checkcif.iucr.org/). Asterisk in ^{1}H-NMR spectra designates the triazole ring proton and we have found this signal to be suppressed in all 1,4-regioisomeric triazole-urea compounds bearing a 2-benzyl (e.g. KT116, KT109, KT172) but not 2-phenyl (e.g. KT195) group.

Synthesis of KT116.

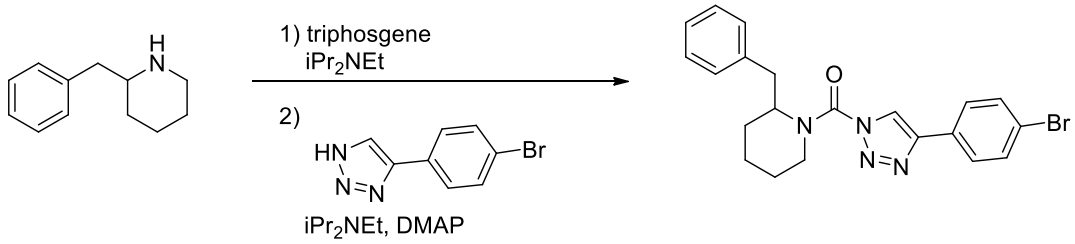

A solution of 2-benzylpiperidine (0.32 g, 1.8 mmol) in THF (15 mL) was treated with iPr_2NEt (0.95 mL, 5.4 mmol) and triphosgene (0.27 g, 0.9 mmol), and the reaction mixture was stirred for 30 min at 4 ^oC. The mixture was poured into H_2O and extracted with ethyl acetate. The organic layer was washed with H_2O and brine, dried over Na_2SO_4 and concentrated under reduced pressure. The intermediate was dissolved in THF (20 mL), and iPr_2NEt (0.95 mL, 5.4 mmol), DMAP (218 mg, 1.8 mmol) and 4-(4-bromophenyl)-1H-1,2,3-triazole (0.40 g, 1.8 mmol) were added to the solution. The mixture was stirred for 2 h at 60 ^oC and poured into saturated aqueous NH_4Cl solution. The mixture was extracted with ethyl acetate, washed with H_2O and brine, dried over

Na_2SO_4 and concentrated under reduced pressure. Chromatography (70 g SiO_2, ethyl acetate:hexane=1:6~1:5) afforded 1,4-triazole urea (320 mg, 42%) as the top TLC spot. ^{1}H NMR ($CDCl_3$, 400 MHz) δ 7.72-7.54 (m, 4H), 7.45-6.89 (m, 6H), 4.81 (bs, 1H), 4.34 (bd, 1H, *J* = 13.5 Hz), 3.42-3.10 (m, 2H), 2.67 (bs, 1H), 2.04-1.60 (m, 6H). ^{13}C NMR ($CDCl_3$, 150 MHz) 150.95, 146.21, 138.82, 132.96, 130.02, 129.57, 129.53, 128.11, 127.43, 123.33, 121.44, 58.25, 41.77, 37.49, 29.79, 26.18, 19.73. HRMS calculated for $C_{21}H_{22}BrN_4O$ $[M+H]^+$ 425.0971, found 425.0976.

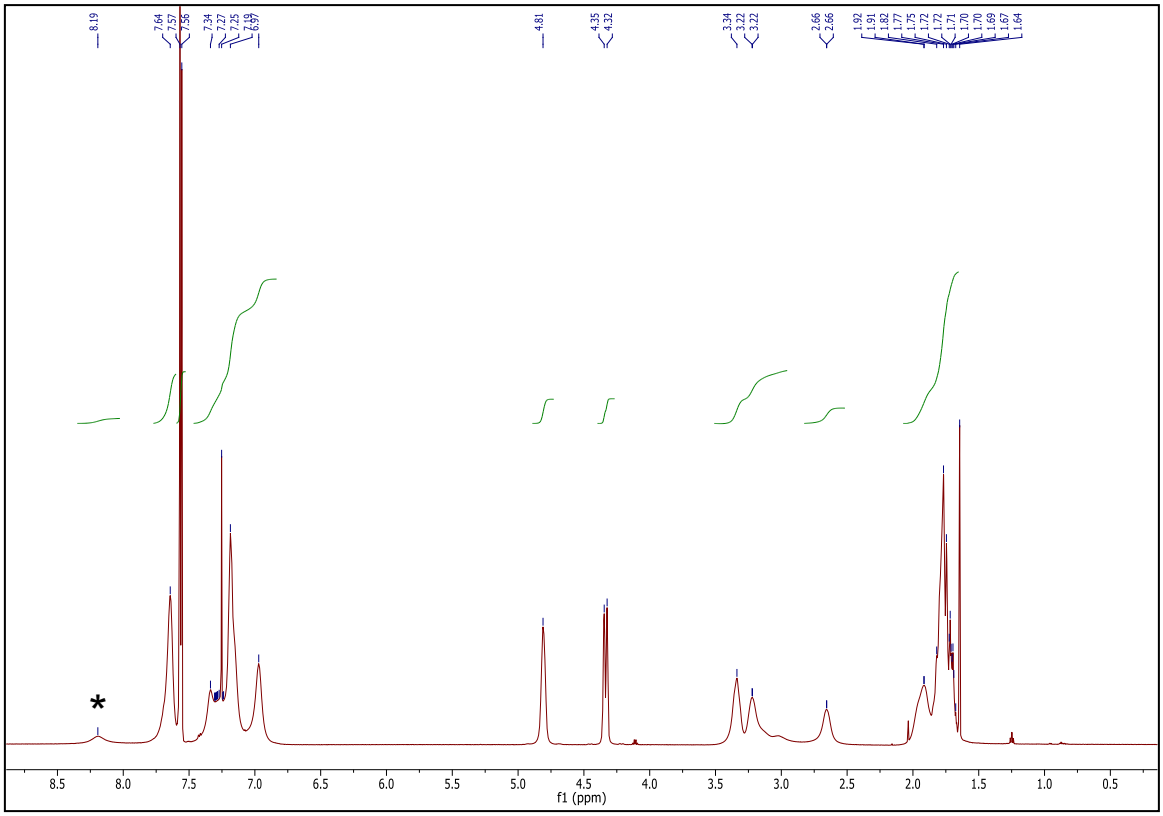

Characterization of KT117.

^{1}H-NMR ($CDCl_3$, 400 MHz): δ = 8.01 (s, 1H), 7.74-7.57 (m, 4H), 7.29-7.07 (m, 5H), 4.61 (bs, 2H), 3.30 (m, 1H), 3.18 (m, 1H), 3.02 (m, 1H), 1.91-1.61 (m, 6H). ^{13}C NMR ($CDCl_3$, 100 MHz) 150.1, 148.3, 138.4, 131.2, 129.5, 128.5, 128.3, 127.0, 123.9, 59.5, 51.1, 36.4, 27.1, 26.9, 25.9. HRMS calculated for $C_{21}H_{22}BrN_4O$ $[M+H]^+$ 425.0972, found 425.0975.

Synthesis of KT109.

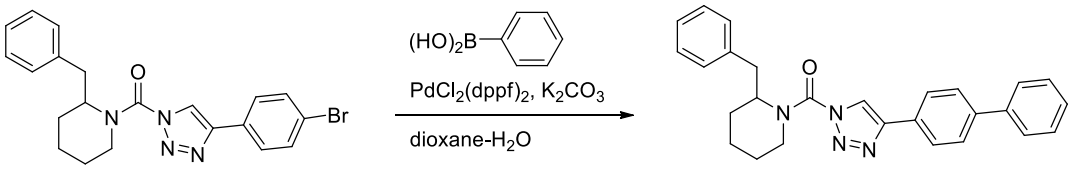

A solution of KT116 (30 mg, 0.071 mmol) in dioxane (2 mL) and H_2O (0.1 mL) was treated with phenylboronic acid (16 mg, 0.13 mmol), K_2CO_3 (30 mg, 0.22 mmol) and $PdCl_2$(dppf) (8.0 mg, 0.011 mmol), and the reaction mixture was stirred for 2 h at 80 ^oC under N_2. The mixture was poured into H_2O and extracted with ethyl acetate. The organic layer was washed with H_2O and brine, dried over Na_2SO_4 and concentrated under reduced pressure. The residue was purified by pTLC (ethyl acetate:hexane=1:4) to afford KT109 (23 mg, 77%).

^{1}H NMR ($CDCl_3$, 400 MHz) δ 7.86 (bs, 2H), 7.70-7.65 (m, 4H), 7.50-7.35 (m, 3H), 7.30-6.90 (m, 5H), 4.87 (bs, 1H), 4.37 (bd, 1H, *J* = 13.7 Hz), 3.40-3.20 (m, 2H), 2.71 (bs, 1H), 2.03-1.65 (m, 6H). ^{13}C NMR ($CDCl_3$, 150 MHz) 150.20, 146.96, 142.13, 141.35, 138.83, 130.04, 129.73, 129.59, 129.51, 128.47, 128.41, 127.88, 127.47, 127.02, 121.36, 58.26, 41.80, 37.51, 29.66, 26.24, 19.75. HRMS calculated for $C_{27}H_{27}N_4O$ $[M+H]^+$ 423.2179, found 423.2178.

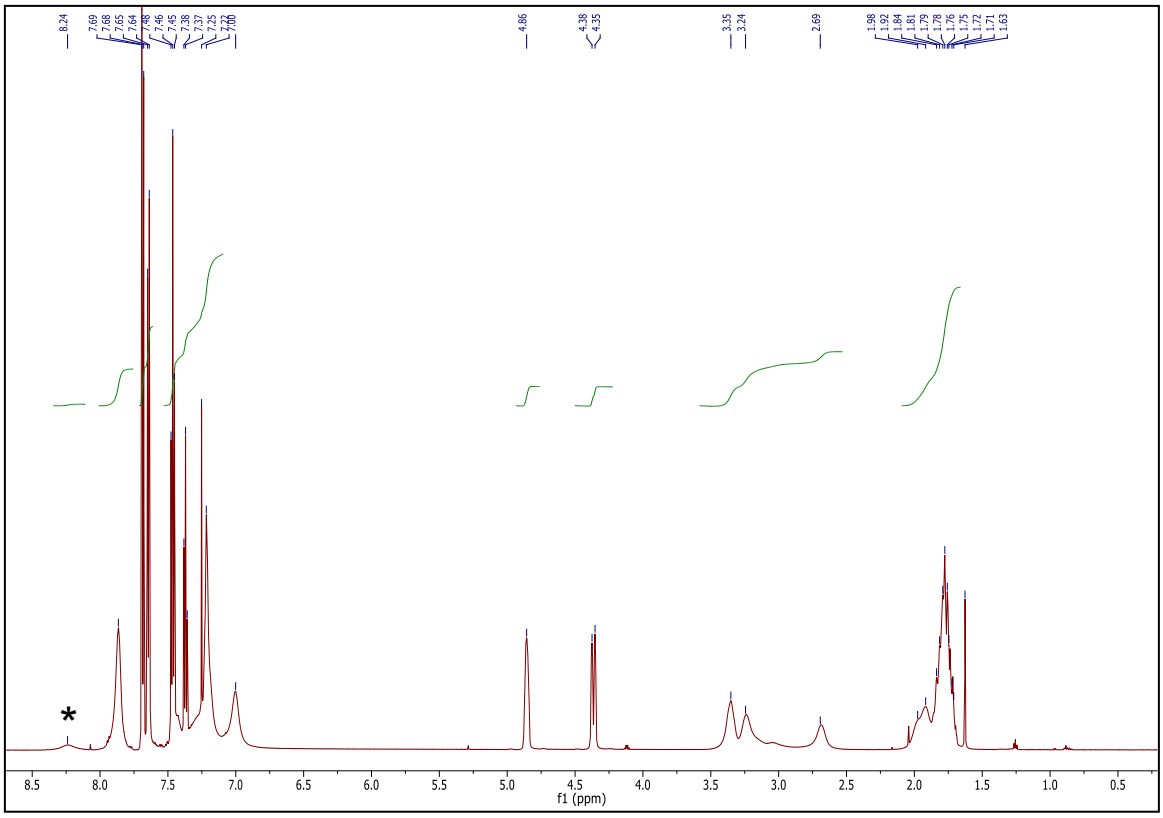

Synthesis of KT172.

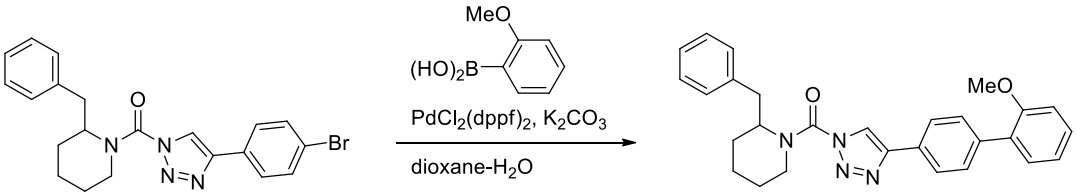

A solution of KT116 (30 mg, 0.071 mmol) in dioxane (2 mL) and H_2O (0.1 mL) was treated with phenylboronic acid (17 mg, 0.13 mmol), K_2CO_3 (30 mg, 0.22 mmol) and $PdCl_2(dppf)$ (8.0 mg, 0.011 mmol), and the reaction mixture was stirred for 2 h at 80 ^oC under N_2. The mixture was poured into H_2O and extracted with ethyl acetate. The organic layer was washed with H_2O and brine, dried over Na_2SO_4 and concentrated under reduced pressure. The residue was purified by pTLC (ethyl acetate:hexane=1:4) to afford KT172 (27 mg, 85%).

^{1}H NMR ($CDCl_3$, 400 MHz) δ 7.84 (bs, 2H), 7.63 (d, 2H, *J* = 8.4 Hz), 7.50-6.95 (m, 9H), 4.87 (bs, 1H), 4.37 (bd, 1H, *J* = 13.8 Hz), 3.84 (s, 3H), 3.42-3.10 (m, 2H), 2.71 (bs, 1H), 2.03-1.65 (m, 6H). ^{13}C NMR ($CDCl_3$, 150 MHz) 157.36, 150.25, 147.20, 138.82, 131.61, 130.92, 130.87, 130.03, 129.75, 129.59, 129.10, 127.49, 126.29, 121.78, 112.13, 58.21, 56.46, 41.79, 37.47, 29.69, 26.25, 19.76. HRMS calculated for $C_{28}H_{29}N_4O_2$ $[M+H]^+$ 453.2285, found 453.2297.

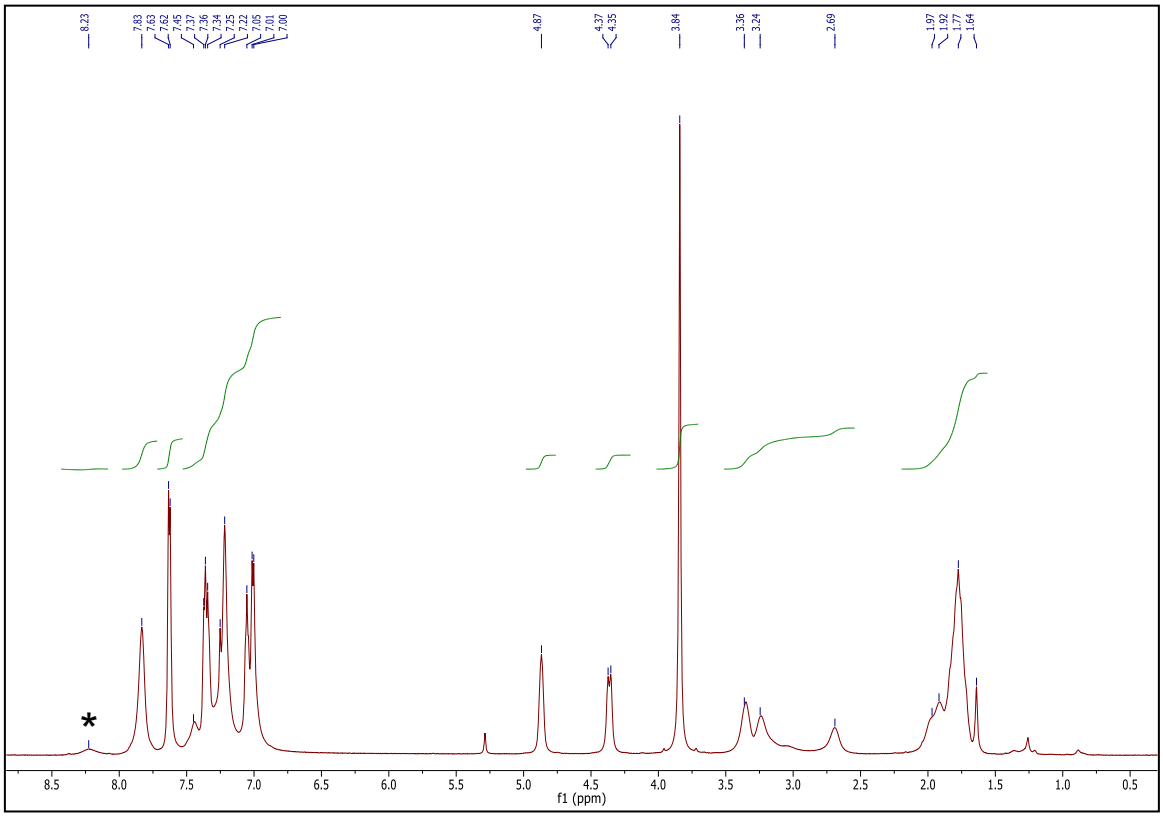

Synthesis of KT179 (**36**).

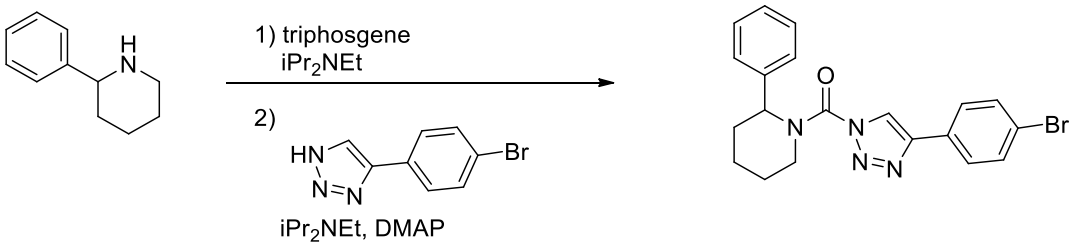

A solution of 2-phenylpiperidine (0.42 g, 2.6 mmol) in THF (8 mL) was treated with iPr_2NEt (1.4 mL, 7.8 mmol) and triphosgene (0.39 g, 1.3 mmol), and the reaction mixture

was stirred for 30 min at 4 °C. The mixture was poured into H_2O and extracted with ethyl acetate. The organic layer was washed with H_2O and brine, dried over Na_2SO_4 and concentrated under reduced pressure. The intermediate was dissolved in THF (10 mL), and iPr_2NEt (1.4 mL, 7.8 mmol), DMAP (0.32 g, 2.6 mmol) and 4-(4-bromophenyl)-1H-1,2,3-triazole (0.60 g, 2.6 mmol) were added to the solution. The mixture was stirred for 2 h at 60 °C and poured into saturated aqueous NH_4Cl solution. The mixture was extracted with ethyl acetate, washed with H_2O and brine, dried over Na_2SO_4 and concentrated under reduced pressure. Chromatography (60 g SiO_2, ethyl acetate:hexane=1:6) afforded 1,4-triazole urea (450 mg, 42%) as the top TLC spot. ^1H NMR ($CDCl_3$, 400 MHz) δ 8.40 (s, 1H), 7.75 (d, 2H, *J* = 8.5 Hz), 7.58 (d, 2H, *J* = 8.5 Hz), 7.43-7.26 (m, 5H), 5.91 (bs, 1H), 4.36 (bd, 1H, *J* = 13.6 Hz), 3.18 (m, 1H), 2.52 (bd, 1H, *J* = 14.2 Hz), 2.15 (m, 1H), 1.90-1.60 (m, 4H). ^{13}C NMR ($CDCl_3$, 150 MHz) 150.15, 146.74, 138.66, 133.03, 129.85, 129.41, 128.27, 128.08, 127.42, 123.55, 122.01, 28.68, 26.67, 20.16. HRMS calculated for $C_{20}H_{20}BrN_4O$ $[M+H]^+$ 411.0815, found 411.0802.

Synthesis of KT195.

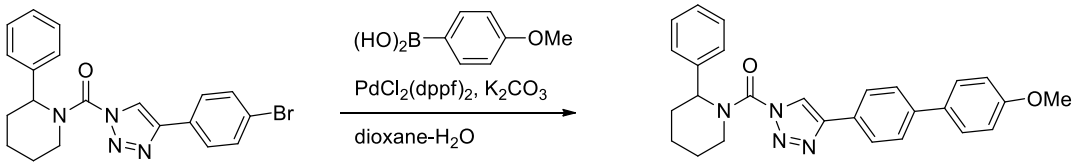

A solution of KT179 (100 mg, 0.24 mmol) in dioxane (4 mL) and H_2O (0.4 mL) was treated with 4-methoxyphenylboronic acid (55 mg, 0.37 mmol), K_2CO_3 (100 mg, 0.72 mmol) and $PdCl_2(dppf)$ (18 mg, 0.024 mmol), and the reaction mixture was stirred for 2 h at 80 °C under N_2. The mixture was poured into H_2O and extracted with ethyl acetate. The organic layer was washed with H_2O and brine, dried over Na_2SO_4 and concentrated under reduced pressure. Chromatography (50 g SiO_2, ethyl acetate:hexane=1:5~1:4) afforded KT195 (70 mg, 66%).

^{1}H NMR ($CDCl_3$, 400 MHz) δ 8.42 (s, 1H), 7.93 (d, 2H, *J* = 8.3 Hz), 7.65 (d, 2H, *J* = 8.3 Hz), 7.58 (d, 2H, *J* = 8.8 Hz), 7.43-7.26 (m, 5H), 7.00 (d, 2H, *J* = 8.8 Hz), 5.94 (bs, 1H), 4.78 (bd, 1H, *J* = 13.8 Hz), 3.86 (s, 3H), 3.19 (bt, 1H, *J* = 13.8 Hz), 2.54 (bd, 1H, *J* = 13.8 Hz), 2.16 (m, 1H), 1.91-1.60 (m, 4H). ^{13}C NMR ($CDCl_3$, 150 MHz) 160.24, 150.34, 147.54, 141.91, 138.76, 133.80, 129.84, 128.91, 128.75, 128.04, 128.02, 127.46, 127.15, 121.71, 115.16, 56.24, 28.69, 26.70, 20.20. HRMS calculated for $C_{27}H_{27}N_4O_2$ $[M+H]^+$ 439.2128, found 439.2128.

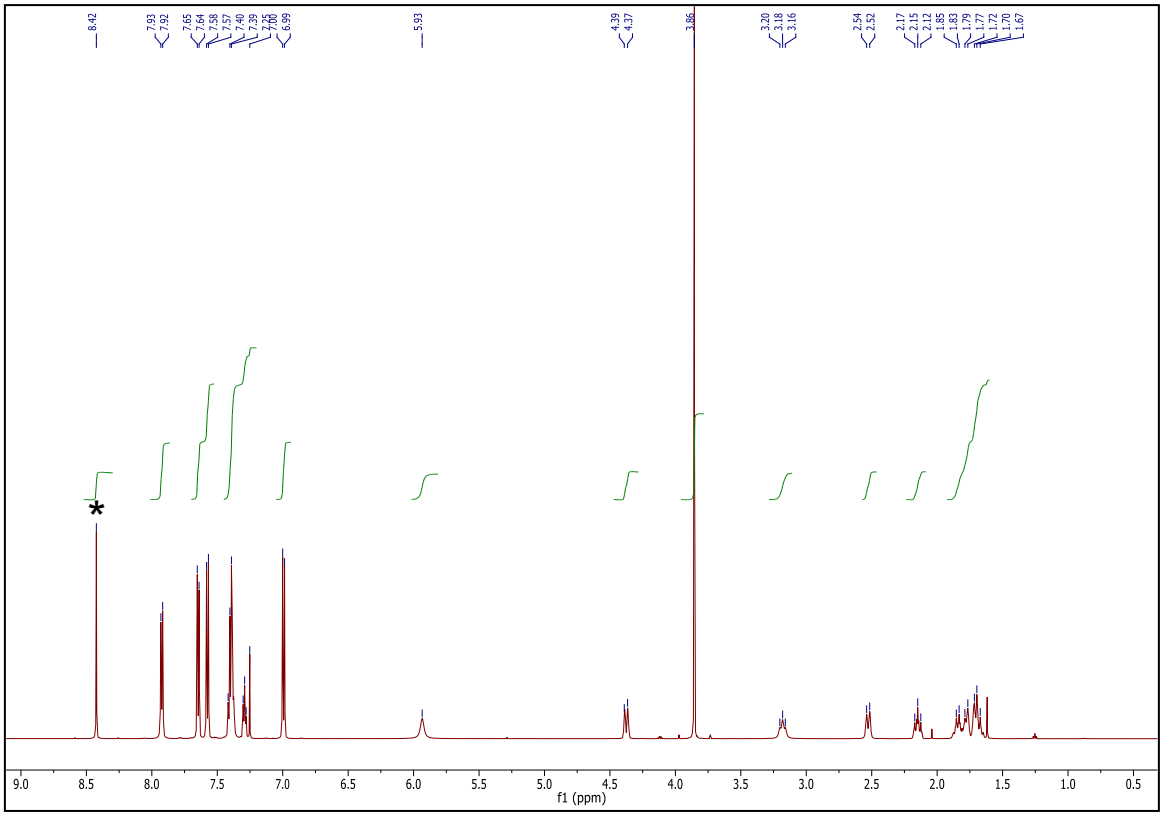

Crystal structure of KT195 (CCDC 901536)

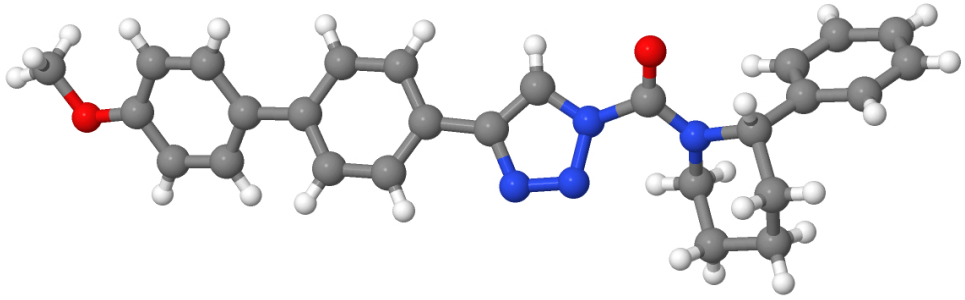

Synthesis of HT-01.

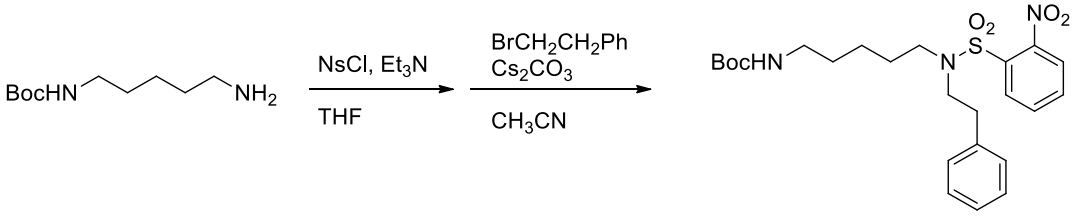

A solution of N-Boc-cadaverine (0.50 g, 2.48 mmol) in THF (10 mL) was treated with *o*-nitrophenylsulfonyl chloride (0.55 g, 2.48 mmol) and Et_3N (0.51 mL, 3.71 mmol), and the mixture was stirred for 1 h at room temperature. The mixture was poured into H_2O and extracted with ethyl acetate. The organic layer was washed with H_2O and brine, dried over Na_2SO_4 and concentrated under reduced pressure. The residue was dissolved in CH_3CN (20 mL), and Cs_2CO_3 (2.40 g, 7.43 mmol) and phenethylbromide (0.69 g, 3.71 mmol) was added. The mixture was stirred for 2 h at 80 ^oC. The mixture was poured into H_2O and extracted with ethyl acetate. The organic layer was washed with H_2O and brine, dried over Na_2SO_4 and concentrated under reduced pressure. Chromatography (50 g SiO_2, ethyl acetate:hexane=1:2) afforded sulfone amide (**37**) (1.1 g, 91%).

^1H NMR ($CDCl_3$, 300 MHz) δ 7.96 (m, 1H), 7.30-7.15 (m, 5H), 4.50 (bs, 1H), 3.50 (m, 2H), 3.33 (t, 2H, *J* = 7.5 Hz), 3.07 (q, 2H, *J* = 6.7 Hz), 2.84 (m, 2H), 1.65-1.38 (m, 4H), 1.44 (s, 9H), 1.34-1.20 (m, 2H). ^{13}C NMR ($CDCl_3$, 100 MHz) 156.33, 148.38, 138.39,

133.98, 133.74, 131.96, 131.03, 129.13, 128.97, 127.03, 124.53, 79.48, 49.15, 47.96, 40.63, 35.48, 29.98, 28.79, 28.10, 24.04. HRMS calculated for $C_{24}H_{34}N_3O_6S$ $[M+H]^+$ 492.2163, found 492.2169.

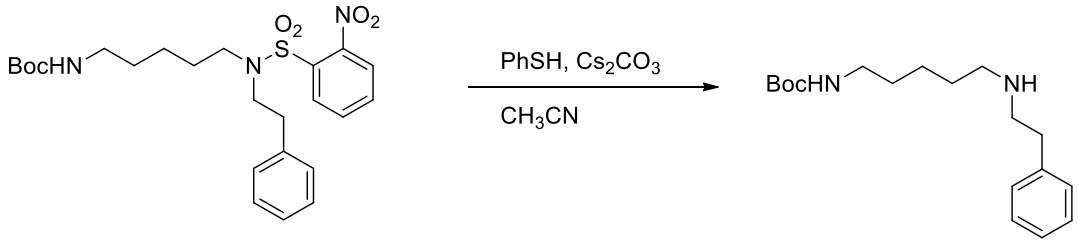

A solution of the sulfone amide (0.70 g, 1.43 mmol) in CH_3CN (15 mL) was treated with Cs_2CO_3 (1.40 g, 4.29 mmol) and benzenethiol (0.22 ml, 2.14 mmol), and the mixture was stirred overnight at room temperature. The mixture was extracted with CH_2Cl_2, and the organic layer was dried over Na_2SO_4 and concentrated under reduced pressure. Chromatography (30 g SiO_2, CH_2Cl_2/MeOH 10/1~ CH_2Cl_2/MeOH/*n*$PrNH_2$ = 100/10/5) afforded amine (**38**) (0.30 g, 69%).

^{1}H NMR ($CDCl_3$, 300 MHz) δ 7.33-7.17 (m, 5H), 4.56 (bs, 1H), 2.93-2.80 (m, 4H), 2.64 (t, 2H, *J* = 7.3 Hz), 2.43 (bs, 1H), 1.57-1.40 (m, 4H), 1.43 (s, 9H), 1.37-1.25 (m, 2H). ^{13}C NMR ($CDCl_3$, 100 MHz) 156.36, 140.23, 129.06, 128.84, 126.55, 79.38, 51.42, 49.92, 40.83, 36.49, 30.28, 29.81, 29.80, 24.86. HRMS calculated for $C_{18}H_{31}N_2O_2$ $[M+H]^+$ 307.2380, found 307.2380.

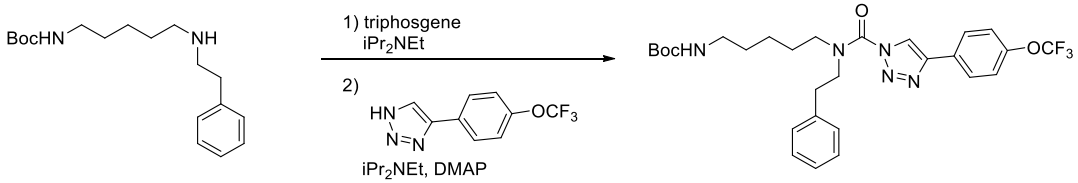

A solution of the amine (78 mg, 0.25 mmol) in THF (3 mL) was treated with iPr_2NEt (0.13 ml, 0.76 mmol) and triphosgene (38 mg, 0.13 mmol), and the reaction mixture was stirred for 30 min at 4 ^{o}C. The mixture was poured into H_2O and extracted with ethyl

acetate. The organic layer was washed with H_2O and brine, dried over Na_2SO_4 and concentrated under reduced pressure. The intermediate was dissolved in THF (4 mL), and iPr_2NEt (0.13 mL, 0.76 mmol), DMAP (30 mg, 0.25 mmol) and 4-(4-trifluoromethoxyphenyl)-1H-1,2,3-triazole (57 mg, 0.25 mmol) were added to the solution. The mixture was stirred for 2 h at 60 ^oC and poured into saturated aqueous NH_4Cl solution. The mixture was extracted with ethyl acetate, washed with H_2O and brine, dried over Na_2SO_4 and concentrated under reduced pressure. Chromatography (30 g SiO_2, ethyl acetate:hexane=1:3) afforded 1,4-triazole urea (**39**) (51 mg, 37%) as the top TLC spot.

^1H NMR ($CDCl_3$, 300 MHz) δ 8.41-7.80 (m, 3H), 7.40-7.10 (m, 7H), 4.57 (bs, 1H), 4.03-3.50 (m, 4H), 3.20-2.95 (m, 4H), 1.84-1.20 (m, 6H), 1.44 (s, 9H). ^{13}C NMR ($CDCl_3$, 150 MHz) 156.90, 150.16, 146.09, 138.55, 129.78, 129.60, 129.21, 128.37, 128.17, 127.49, 122.32, 122.16, 121.86, 121.30 (q, J = 257.5 Hz, OCF_3), 80.05, 52.14, 50.05, 41.16, 35.95, 30.66, 29.28, 27.76, 24.84. HRMS calculated for $C_{28}H_{35}F_3N_5O_4$ $[M+H]^+$ 562.2636, found 562.2628.

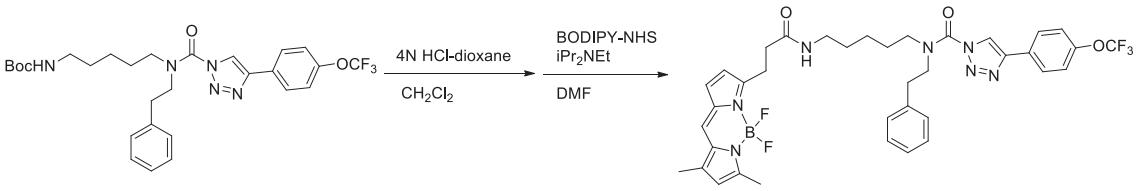

A solution of the urea (7.2 mg, 12.8 mmol) in CH_2Cl_2 (0.5 mL) was treated with 4N HCl-dioxane (0.5 mL), and the mixture was stirred for 3 h at room temperature. The solvent was evaporated and the residue was dissolved in DMF (0.8 mL). iPr_2NEt (7 μl, 38.6 μmol) and BODIPY-NHS (5.0 mg, 12.8 μmol) was added to the solution, and the mixture was stirred overnight at room temperature. The mixture was poured into H_2O and extracted with ethyl acetate. The organic layer was washed with H_2O and brine, dried

over Na_2SO_4 and concentrated under reduced pressure. pTLC (ethyl acetate:hexane=3:1) afforded HT-01 (6 mg, 64%).

^{1}H NMR ($CDCl_3$, 400 MHz) δ 8.42-7.80 (m, 3H), 7.32-7.10 (m, 7H), 6.88 (bs, 1H), 6.28 (bs, 1H), 6.10 (s, 1H), 5.84 (bs, 1H), 3.96 (bs, 1H), 3.72 (m, 1H), 3.59-3.48 (m, 2H), 3.30-2.93 (m, 6H), 2.63 (t, 2H, *J* = 7.5 Hz), 2.50 (s, 3H), 2.23 (s, 3H), 1.78-1.20 (m, 6H).

^{13}C NMR ($CDCl_3$, 150 MHz) 172.56, 161.07, 158.26, 150.14, 146.08, 144.80, 138.56, 135.96, 134.22, 129.78, 129.61, 129.18, 128.16, 127.49, 124.70, 122.90, 122.05, 121.85, 121.31, 121.32 (q, *J* = 257.5 Hz, OCF_3), 118.37, 52.10, 49.87, 40.06, 36.90, 35.92, 29.86, 27.67, 25.83, 24.80, 15.81, 12.17. HRMS calculated for $C_{37}H_{40}BF_5N_7O_3$ $[M+H]^+$ 736.3200, found 736.3204.

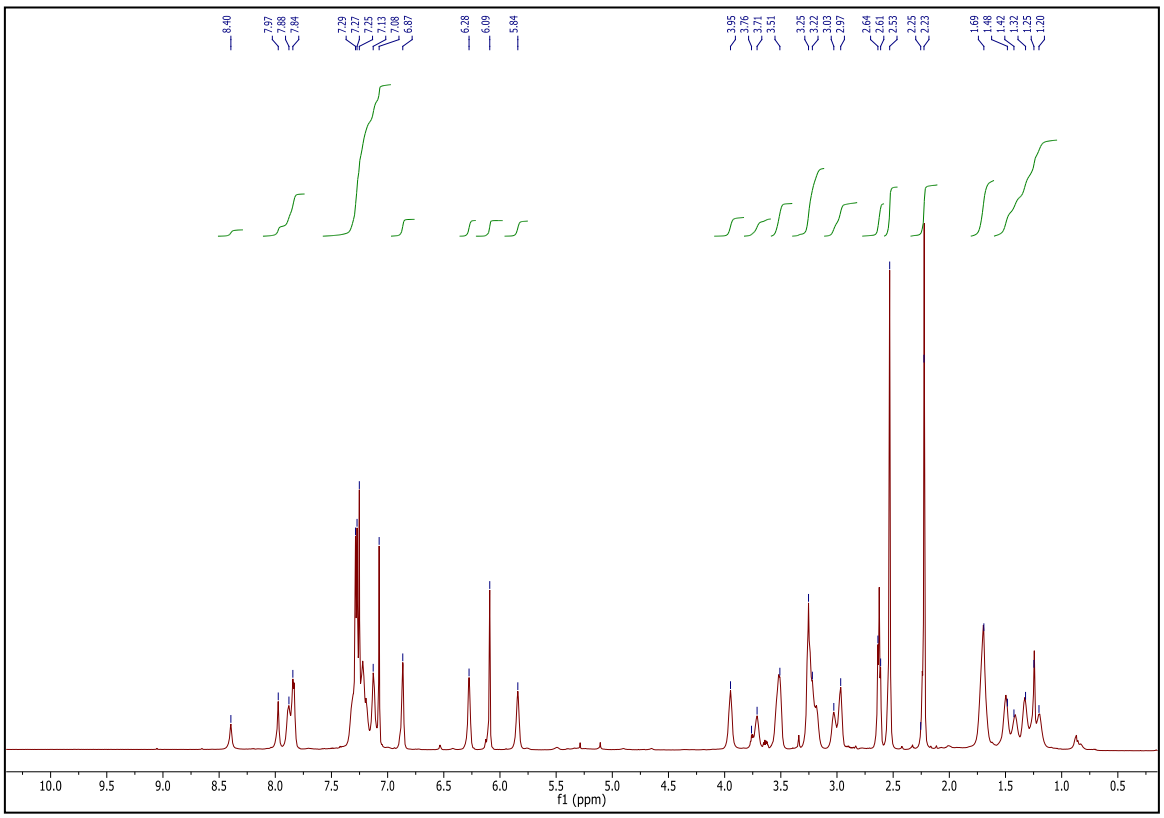

References

1 Bonventre, J. V. *et al.* Reduced fertility and postischaemic brain injury in mice deficient in cytosolic phospholipase A2. *Nature* **390**, 622-625 (1997).

2 Liu, Y., Patricelli, M. P. & Cravatt, B. F. Activity-based protein profiling: the serine hydrolases. *Proc. Natl. Acad. Sci. U S A* **96**, 14694-14699 (1999).

3 Gao, Y. *et al.* Loss of Retrograde Endocannabinoid Signaling and Reduced Adult Neurogenesis in Diacylglycerol Lipase Knock-out Mice. *J. Neurosci.* **30**, 2017-2024 (2010).

4 Deems, R., Buczynski, M. W., Bowers-Gentry, R., Harkewicz, R. & Dennis, E. A. Detection and quantitation of eicosanoids via high performance liquid chromatography-electrospray ionization-mass spectrometry. *Methods Enzymol.* **432**, 59-82 (2007).

5 Long, J. Z. *et al.* Selective blockade of 2-arachidonoylglycerol hydrolysis produces cannabinoid behavioral effects. *Nat. Chem. Biol.* **5**, 37-44 (2009).

6 Bachovchin, D. A. *et al.* Superfamily-wide portrait of serine hydrolase inhibition achieved by library-versus-library screening. *Proc. Natl. Acad. Sci. U S A* **107**, 20941-20946 (2010).

7 Jessani, N. *et al.* A streamlined platform for high-content functional proteomics of primary human specimens. *Nat. Methods* **2**, 691-697 (2005).

8 Alexander, J. P. & Cravatt, B. F. Mechanism of carbamate inactivation of FAAH: implications for the design of covalent inhibitors and in vivo functional probes for enzymes. *Chem. Biol.* **12**, 1179-1187 (2005).

9 Schlosburg, J. E. *et al.* Chronic monoacylglycerol lipase blockade causes functional antagonism of the endocannabinoid system. *Nat. Neurosci.* **13**, 1113-1119 (2010).

10 Ahn, K. *et al.* Discovery and characterization of a highly selective FAAH inhibitor that reduces inflammatory pain. *Chem. Biol.* **16**, 411-420 (2009).

11 Li, W., Blankman, J. L. & Cravatt, B. F. A functional proteomic strategy to discover inhibitors for uncharacterized hydrolases. *J. Am. Chem. Soc.* **129**, 9594-9595 (2007).

12 Hoover, H. S., Blankman, J. L., Niessen, S. & Cravatt, B. F. Selectivity of inhibitors of endocannabinoid biosynthesis evaluated by activity-based protein profiling. *Bioorg. Med. Chem. Lett.* **18**, 5838-5841 (2008).

13 Adibekian, A. *et al.* Confirming target engagement for reversible inhibitors in vivo by kinetically tuned activity-based probes. *J. Am. Chem. Soc.* **134**, 10345-10348 (2012).

14 Adibekian, A. *et al.* Click-generated triazole ureas as ultrapotent in vivo–active serine hydrolase inhibitors. *Nat. Chem. Biol.* **7**, 469-478 (2011).

15 Balsinde, J. & Dennis, E. A. Distinct roles in signal transduction for each of the phospholipase A2 enzymes present in P388D1 macrophages. *J. Biol. Chem.* **271**, 6758-6765 (1996).

16 Bachovchin, D. A. *et al.* Academic cross-fertilization by public screening yields a remarkable class of protein phosphatase methylesterase-1 inhibitors. *Proc. Natl. Acad. Sci. U S A* **108**, 6811-6816 (2011).

SUPPLEMENTARY RESULTS

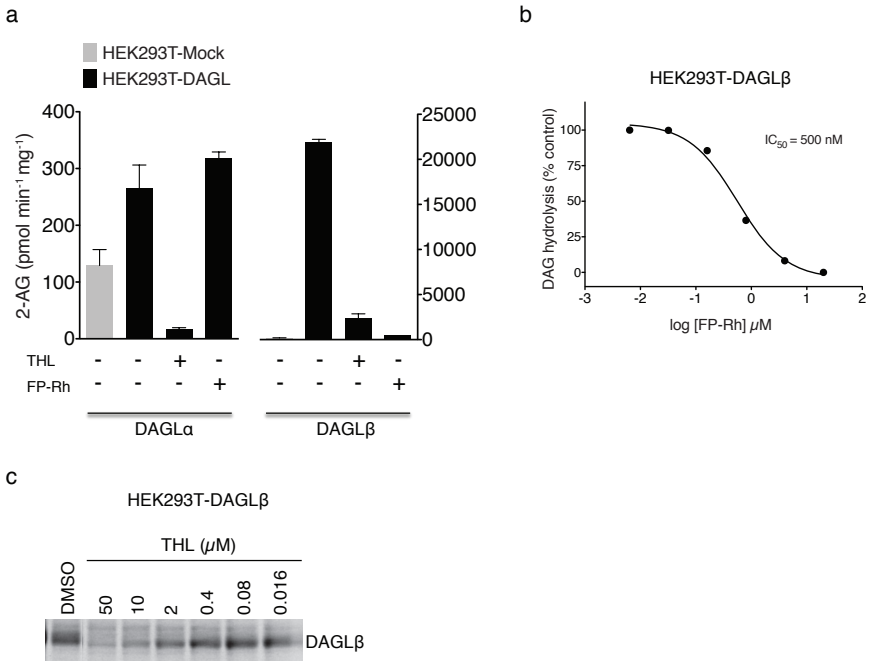

Supplementary Figure 1. Recombinant expression and inhibition of DAGL enzymes in HEK293T cells. (**a**). Activity of recombinant DAGL enzymes expressed by transient transfection in HEK293T cells. Membrane proteomes from DAGLα- or DAGLβ-transfected cells were preincubated with FP-Rh (20 μM) or the non-specific lipase inhibitor, THL (20 μM) for 30 min at 37 ºC. SAG substrate was added to proteomes (500 μM final concentration, 30 min, 37 ºC), reactions quenched with 2:1 v/v $CHCl_3$:MeOH doped with 1-monopentadecanoin standard and hydrolysis products quantified by LC-MS. Data are presented as means ± s.e.m. for two independent experiments. (**b**) Concentration dependent inhibition of DAGLβ by FP-Rh as measured using the LC-MS substrate assay described in part (**a**). Data are presented as means ± s.e.m. for two independent experiments. 95% confidence intervals for IC_{50} value for FP-Rh: 0.4 to 0.7 μM. (**c**) Gel-based competitive ABPP assay for DAGLβ. HEK293T-DAGLβ membrane lysate (0.3 mg/mL) was preincubated with varying concentrations of THL for 30 min at 37 ºC. Proteomes were then labeled with the activity-based probe, FP-Rh (5 μM, 30 min, 37 ºC) and separated by SDS-PAGE. DAGLβ activity was detected by in-gel fluorescence scanning. Inhibition of DAGLβ was detected by reduced probe-labeling. This gel and subsequent fluorescent gels are shown in grayscale.

Number	ID	Structure
1	AA26-1	
2	AA26-2	
3	AA26-3	
4	AA26-4	
5	AA26-5	
6	AA26-6	
7	AA26-7	
8	AA26-8	
9	AA26-9	
10	AA32-1	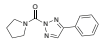

Number	ID	Structure
11	AA32-2	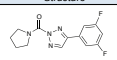
12	AA32-3	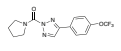
13	AA32-4	
14	AA34-1	
15	AA34-2	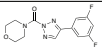
16	AA34-3	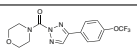
17	AA38-3	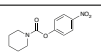
18	AA39-3	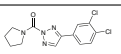
19	AA39-1	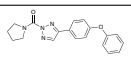
20	AA39-2	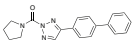

Number	ID	Structure
21	AA39-4	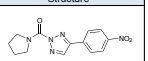
22	AA39-5	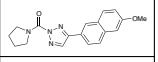
23	AA40-2	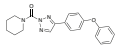
24	AA40-3	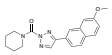
25	KT117	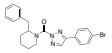
26	AA44-2	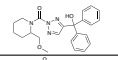
27	AA47-1	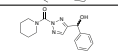
28	AA72-1	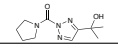
29	AA72-2	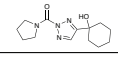
30	AA26-10	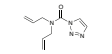

Supplementary Figure 2. Structures of 1,2,3-TUs screened against DAGLβ by gel-based competitive ABPP. Full characterization of compounds can be found in a previous report[14].

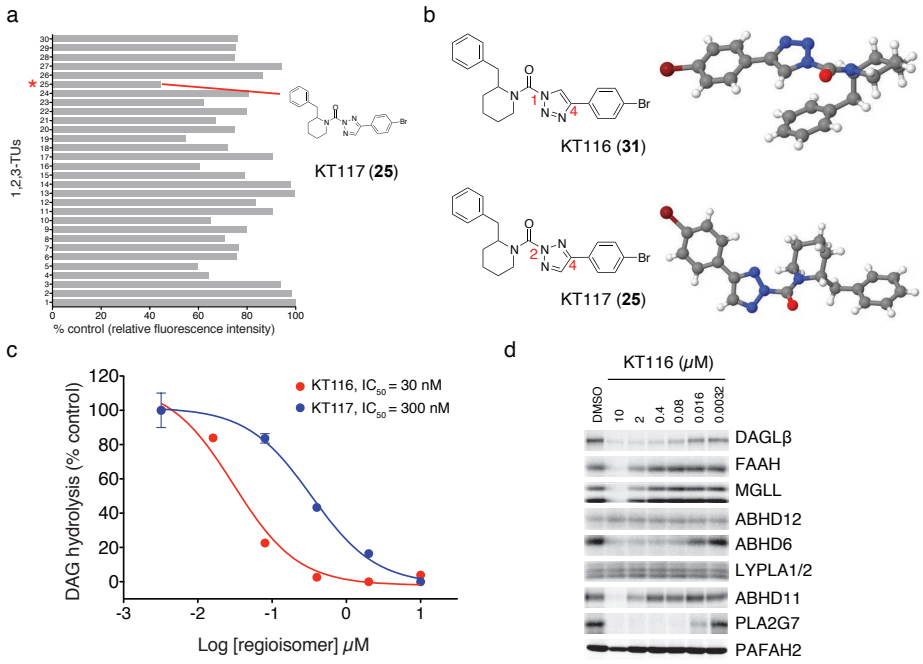

Supplementary Figure 3. Discovery of lead 1,2,3-TU inhibitors for DAGLβ. (**a**) Screening results for a set of 1,2,3-TUs (see **Supplementary Figure 2** for structures) against recombinant mouse DAGLβ. Compounds were preincubated with HEK293T-DAGLβ membrane lysate for 30 min at 37 ºC prior to treatment with the activity-based probe FP-Rh (5 μM, 30 min, 37 ºC) and analysis by gel-based ABPP, where compound activity was measured by reductions in FP-Rh labeling of DAGLβ. Compound KT117 was the most active compound, blocking FP-Rh labeling of DAGLβ by ~60%. (**b**) Chemical and crystal structures of the 1,4- (KT116, CCDC 901535) and 2,4-regioismers (KT117) of the lead DAGLβ inhibitor. (**c**) *In vitro* IC_{50} values for DAGLβ inhibition by KT116 and KT117 as measured with the substrate, 1-stearoyl, 2-arachidonoyl (C18:0/C20:4) DAG (SAG). Inhibitors were pre-incubated with HEK293T-DAGLβ membrane lysate for 30 min at 37 ºC prior to LC-MS-based substrate assay. Data are presented as means ± s.e.m. for two independent experiments. 95% confidence intervals for IC_{50} values (KT116: 20 to 50 nM; KT117: 200 to 600 nM). (**d**) Competitive ABPP of KT116 against a panel of serine hydrolases detected in mouse brain proteome (FAAH, MGLL, ABHD12, ABHD6, LYPLA1/2) or as enzymes recombinantly expressed in HEK293T cells (DAGLβ, ABHD11, PLA2G7, and PAFAH2). Proteomes were treated with compounds and FP-Rh probe as described in part (**a**) except 1 μM FP-Rh was used for profiling enzymes other than DAGLβ.

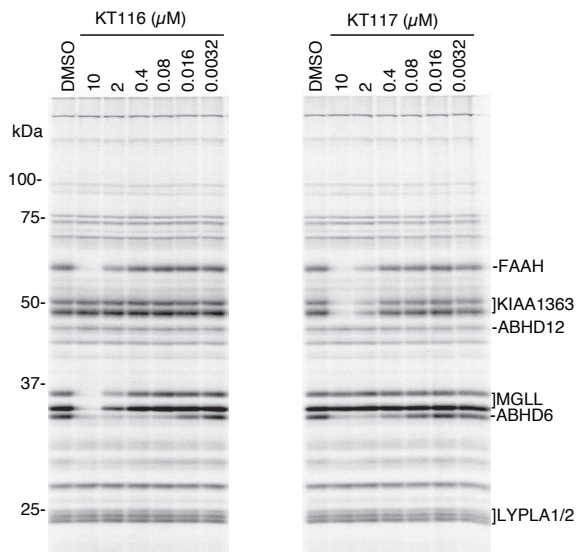

Supplementary Figure 4. Competitive ABPP of KT116 and KT117 with a mouse brain proteome. A mouse brain proteome was incubated with varying concentrations of KT116 or KT117 for 30 min at 37 ºC. Proteomes were then labeled with FP-Rh (1 μM, 30 min, 37 ºC) and separated by SDS-PAGE. FP-Rh-labeled brain serine hydrolases that have been identified in previous studies are marked. See **Supplementary Methods** for more details.

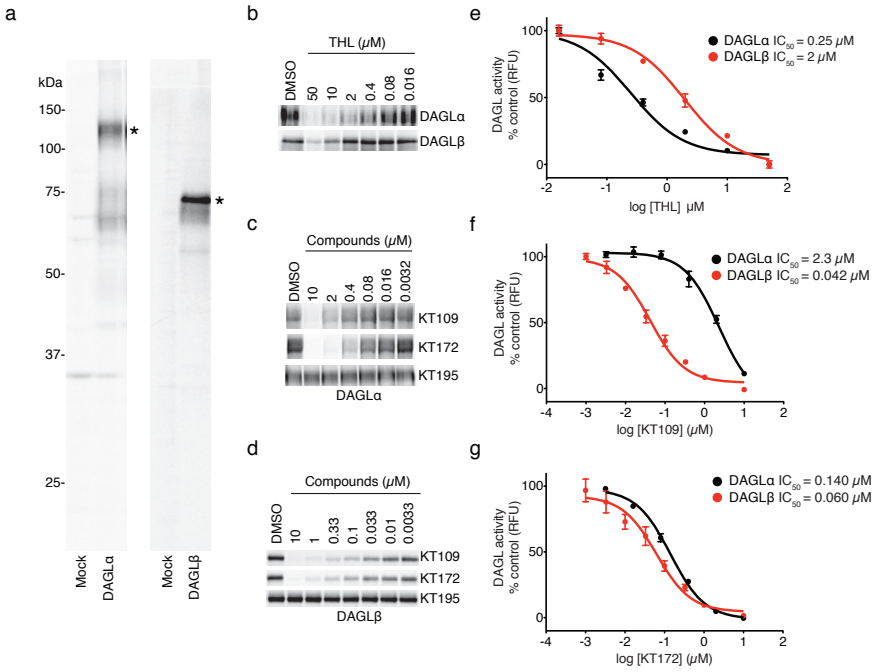

Supplementary Figure 5. Competitive ABPP of recombinant DAGL enzymes using the HT-01 activity-based probe. (**a**) Both DAGLα and DAGLβ activity can be detected in transfected HEK293T cell proteomes by HT-01 (1 μM). (**b-d**) Concentration-dependent inhibition profiles for THL (**b**), KT109 (**c, d**), KT172 (**c, d**), and KT195 (**c, d**) against DAGLα and DAGLβ as measured by competitive ABPP using the HT-01 probe. HEK293T-DAGLα membrane lysates (2 mg/mL) were preincubated with varying concentrations of compound for 30 min at 37 ºC. Proteomes were then labeled with HT-01 (1 μM, 30 min, 37 ºC) and separated by SDS-PAGE, and DAGL activity measured by in-gel fluorescence scanning. Calculated IC_{50} values for DAGLα and DAGLβ inhibition are shown in **e-g**. 95% confidence intervals for DAGLα IC_{50} values (THL: 0.1 to 0.4 μM; KT109: 1.5 to 3.5 μM; KT172: 0.1 to 0.2 μM); DAGLβ IC_{50} values (THL: 1.3 to 2.9 μM; KT109: 0.03 to 0.06 μM; KT172: 0.04 to 0.1 μM). Data are presented as means ± s.e.m.; *n* = 3 experiments per group.

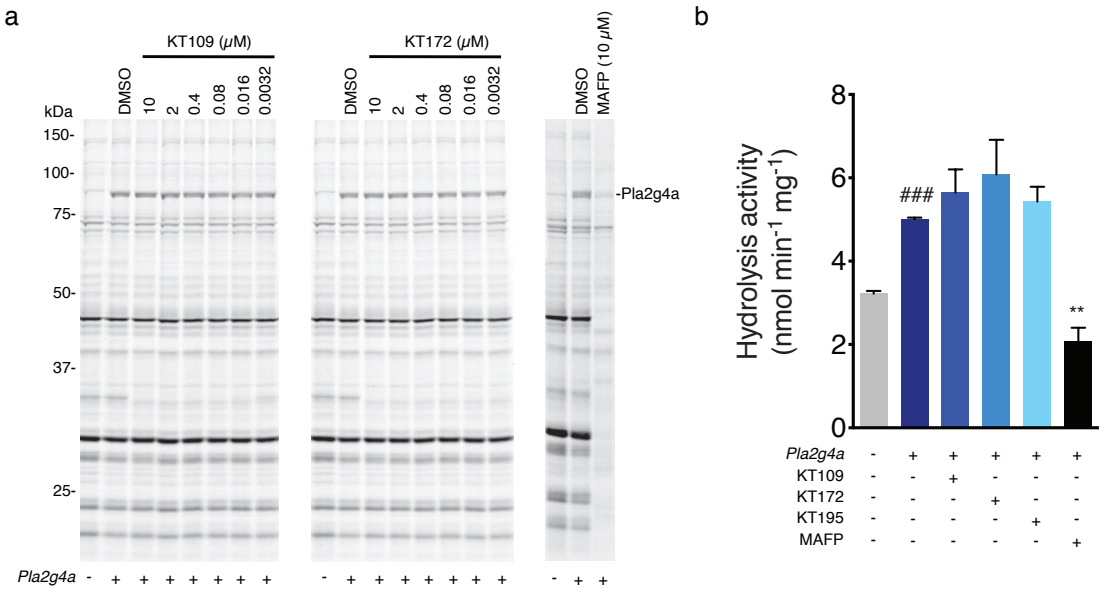

Supplementary Figure 6. Activity of KT109, KT172, and KT195 against recombinant PLA2G4A. KT109, KT172, and KT195 do not inhibit recombinant PLA2G4A overexpressed in HEK293T cells as judged by competitive ABPP (**a**) or by a radiolabeled TLC substrate assay (**b**) that monitored the conversion of [^{14}C-arachdonoyl] 1-stearoyl-2-arachidonoyl-sn-glycerol-3-phosphocholine (PAPC) to arachidonic acid (AA). For competitive ABPP experiments, HEK293T-PLA2G4A overexpressed lysates (1 mg/mL) were preincuabted with varying concentrations of compound for 30 min at 37 ºC. Proteomes were then labeled with FP-Rh (1 μM, 30 min, 37 ºC) and separated by SDS-PAGE and PLA2G4A activity measured by in-gel fluorescence scanning. For both assays, the known PLA2G4A inhibitor methoxy arachidonyl fluorophosphonate (MAFP)[15] was used as a positive control. The radioactive TLC substrate assay was performed as previously described[5].

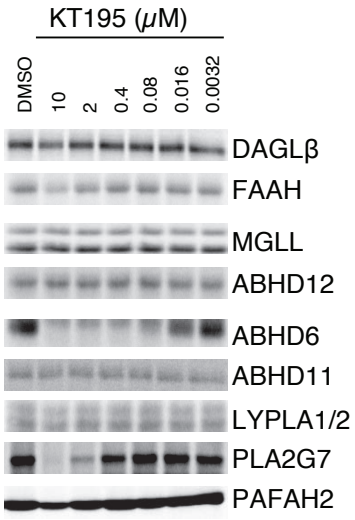

Supplementary Figure 7. Selectivity of KT195 against representative serine hydrolases. Competitive ABPP of KT195 against a panel of serine hydrolases detected in mouse brain proteome (FAAH, MGLL, ABHD12, ABHD6, LYPLA1/2) or as enzymes recombinantly expressed in HEK293T cells (DAGLβ, ABHD11, PLA2G7, and PAFAH2). Proteomes were pre-incubated with indicated concentrations of KT195 for 30 min at 37 ºC and then labeled with 1 μM or 5 μM (for DAGLβ) of FP-Rh (30 min, 37 ºC), separated by SDS-PAGE and labeled proteins detected by in-gel fluorescence scanning.

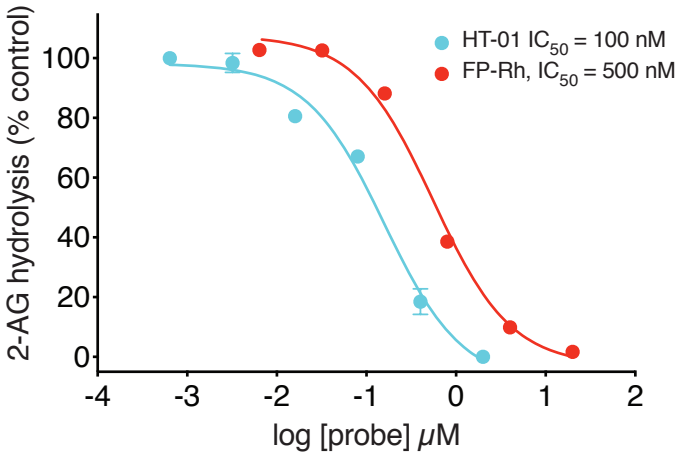

Supplementary Figure 8. *In vitro* IC_{50} values for DAGLβ inhibition by HT-01 and FP-Rh. The activity of probes was measured with the SAG substrate assay following the protocol described in **Supplementary Fig. 3c**. Data are presented as means ± s.e.m. for two independent experiments. 95% confidence intervals for IC_{50} values (HT-01: 100 to 200 nM; FP-Rh: 400 to 700 nM).

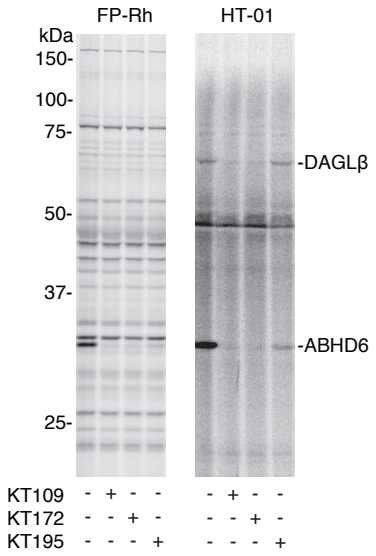

Supplementary Figure 9. Competitive ABPP of KT109, KT172, and KT195 in primary mouse neurons. Profiling primary cortical mouse neuron proteomes (derived from E16-E18 embryos) using FP-Rh (1 μM) or HT-01 (1μM) probes. Proteomes were incubated with probes for 30 min at 37 ºC, separated by SDS-PAGE, and serine hydrolase activities detected by in-gel fluorescence scanning. HT-01 labeling of a 70 kDa protein was inhibited by KT109 (2 μM) and KT172 (2 μM), but not KT195 (2 μM), while HT-01 labeling of a 30 kDa protein was blocked by all three inhibitors. These inhibitor sensitivity profiles and molecular masses match those expected for DAGLβ and ABHD6, respectively (see **Figures 2** and **4** for more details).

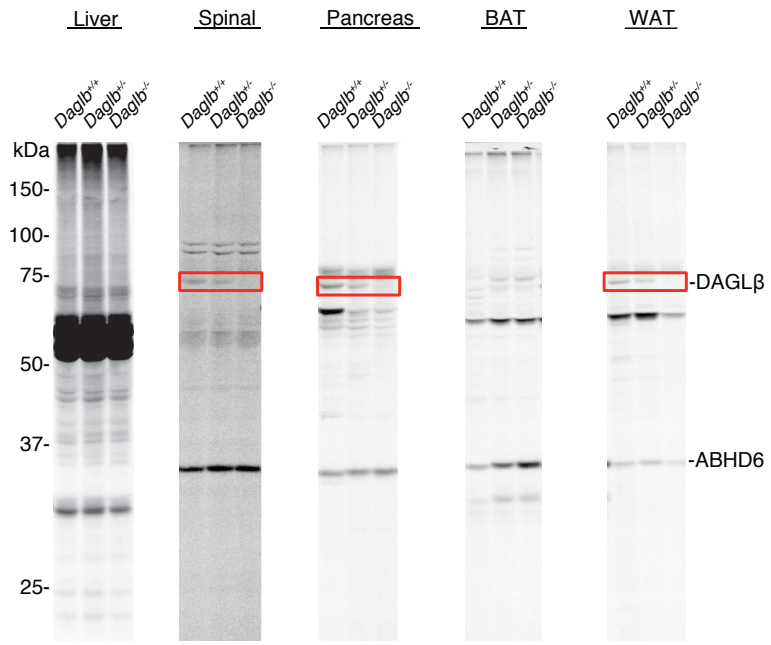

Supplementary Figure 10. Profiling DAGLβ activity in mouse tissues using HT-01. Tissue proteomes from *Daglb*$^{+/+}$, *Daglb*$^{+/-}$, *Daglb*$^{-/-}$ mice were labeled with HT-01 (1 μM) for 30 min at 37 ºC, separated by SDS-PAGE, and HT-01-labeled proteins detected by in-gel fluorescence scanning. DAGLβ (~70 kDa band) activity was detected in spinal, pancreas, and white adipose tissue (WAT) of *Daglb*$^{+/+}$ but not *Daglb*$^{-/-}$ mice (highlighted in red box). DAGLβ could not be detected by HT-01 in liver or brown adipose tissue (BAT), although overlapping signals from other HT-01-labeled serine hydrolases could have obscured DAGLβ detection in the liver proteome.

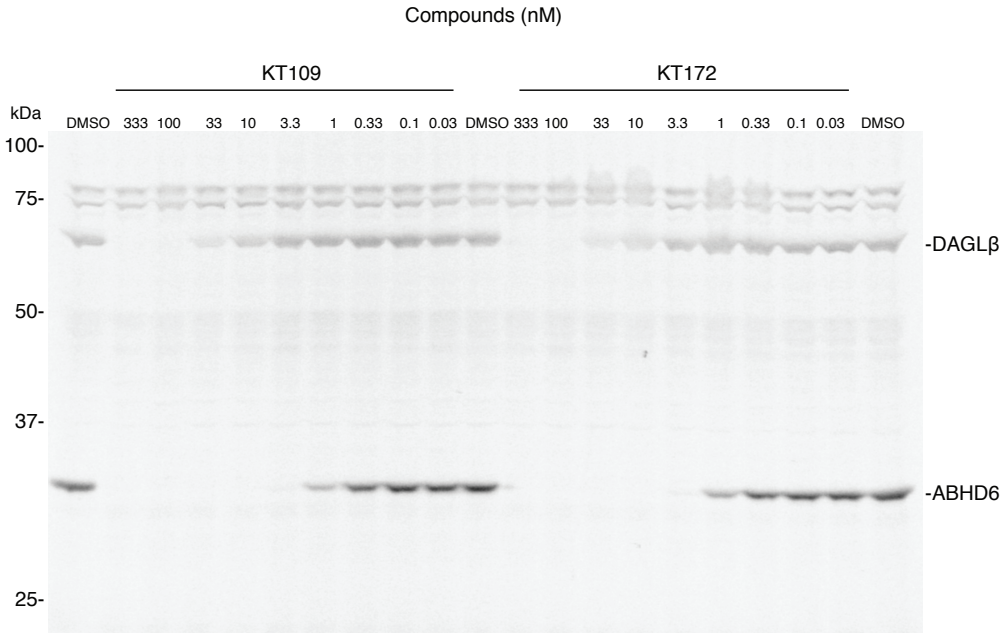

Supplementary Figure 11. *In situ* selectivity profiles of KT109 and KT172 in Neuro2A cells. Neuro2A cells were treated with varying concentrations of compound (333 – 0.03 nM, 4h), lysed, and membrane fractions analyzed by competitive ABPP with HT-01 (1 μM). The IC_{50} of KT109 and KT172 against ABHD6 in Neuro2A cells is ~1 nM.

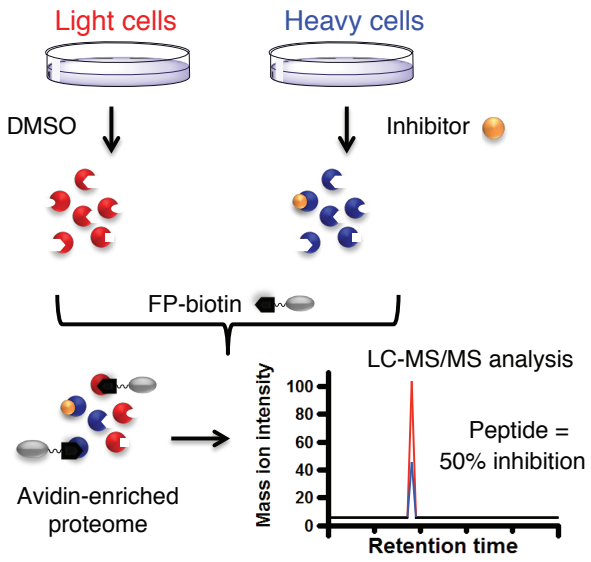

Supplementary Figure 12. Schematic of the competitive ABPP-SILAC platform. Details of the experimental assay are described in the **Methods** and **Supplementary Methods** sections as well as in previous reports[14,16].

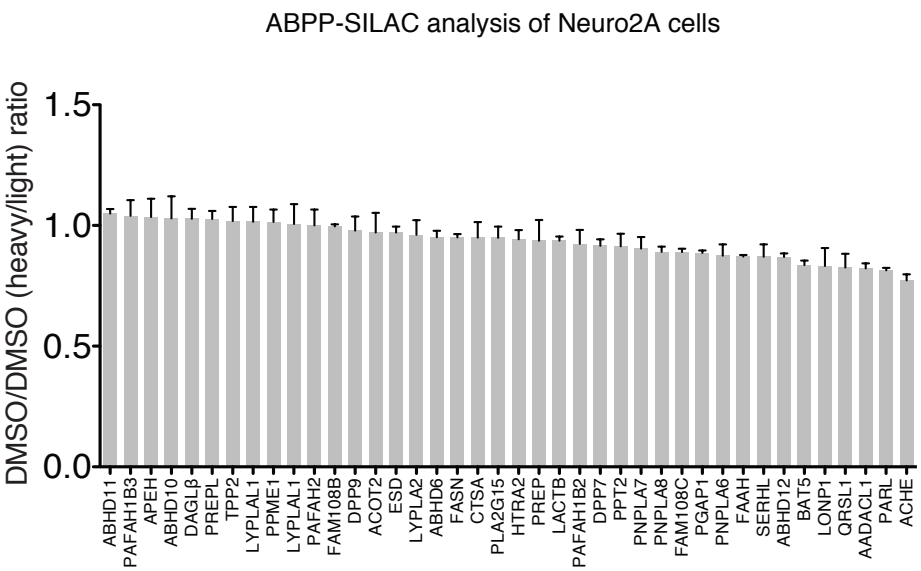

Supplementary Figure 13. ABPP-SILAC analysis of Neuro2A cells. Neuro2A cells grown in “light” and “heavy” media were both treated with DMSO for 4 hr and subjected to ABPP-SILAC analysis. This control experiment confirmed that serine hydrolase activities in Neuro2A cells are not affected by isotopically-labeled media (heavy/light ratios for 40 serine hydrolases were ~1). Bars represent means $\pm$ s.e.m. of heavy/light ratios for the multiple peptides observed for each enzyme (minimum of 2 unique peptides) in both soluble and membrane fractions.

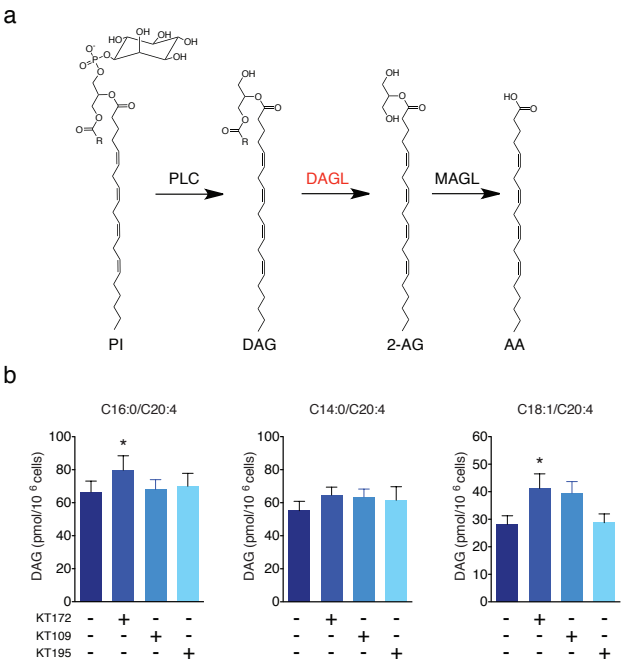

Supplementary Figure 14. Diacylglycerol (DAG) levels in inhibitor-treated Neuro2A cells. (**a**) Current model showing the central role that DAGL enzymes are proposed to play in 2-AG biosynthesis. (**b**) Inhibition of DAGLβ in Neuro2A cells with KT109 or KT172 (50 and 25 nM respectively, 4 h) but not KT195 (25 nM, 4 h) results in modest, but significant increases in C16:0/C20:4 and C18:1/C20:4, but no changes in C14:0/C20:4 DAGs. Data are presented as means ± s.e.m.; *n* = 5-6 mice per group. **P* < 0.05 for inhibitor-treated versus DMSO-treated cells.

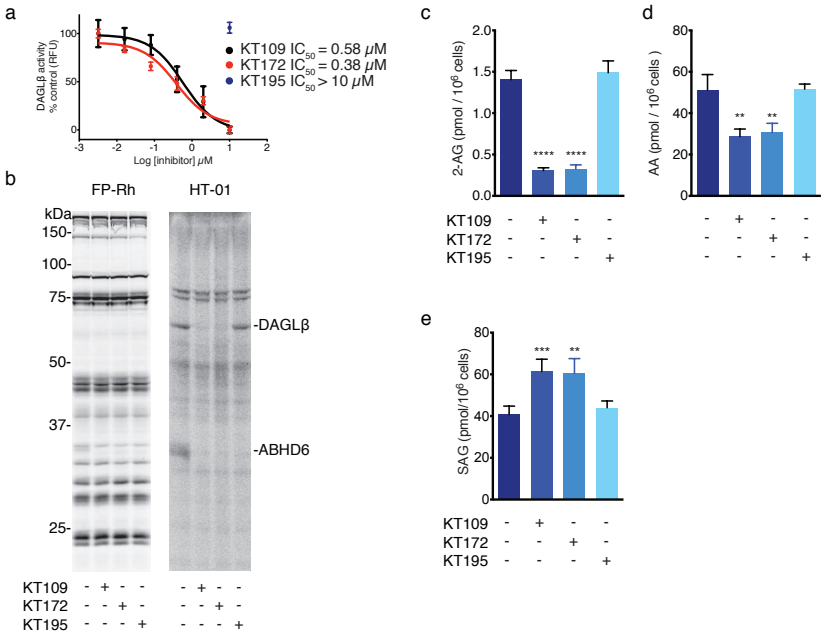

Supplementary Figure 15. Activity of KT109, KT172, and KT195 in human PC3 prostate cancer cells. (**a**) Concentration-dependent inhibition of human DAGLβ activity in PC3 proteomes by KT109 and KT172, but not KT195, as measured by competitive ABPP with the HT-01 probe (1 μM) following the protocol described in **Supplementary Fig. 5.** 95% confidence intervals for IC_{50} values (KT109: 0.2 to 2 μM; KT172: 0.2 to 0.9 μM). (**b-e**) KT109 and KT172, but not KT195, inhibit DAGLβ activity in PC3 cells [*in situ* treatment with inhibitors (100 nM, 4 h)] as measured by competitive ABPP (**b**) and reduce the levels of 2-AG (**c**), AA (**d**), and increase the levels of SAG (**e**) compared with DMSO-treated control cells. Data are presented as means ± s.e.m.; *n* = 5-6 per group. $^{**}p < 0.01$; $^{***}p < 0.001$; $^{****}p < 0.0001$ for inhibitor versus DMSO-treated cells.

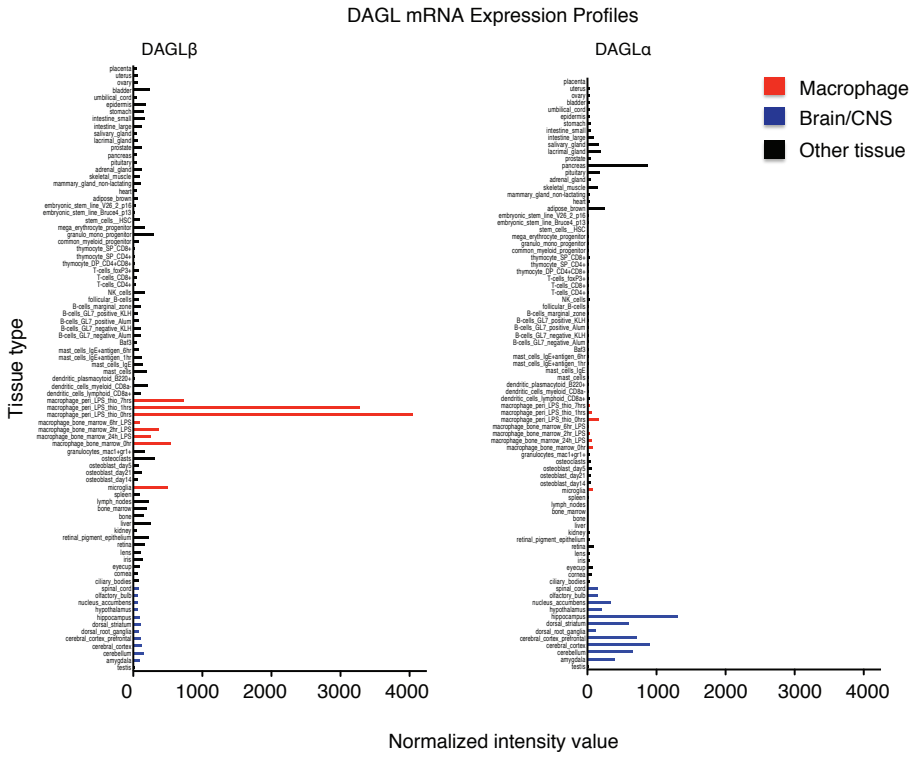

Supplementary Figure 16. Gene expression profiles of DAGL enzymes in mouse tissues and cells. Gene expression profiles were downloaded from the BioGPS database (http://biogps.gnf.org/). DAGLβ is expressed at significantly higher levels in macrophage cell types (red bars) compared to other cell/tissue types (blue and black bars), while DAGLα is most highly expressed in the brain/central nervous system (blue bars) compared to other cell/tissue types (red and black bars).

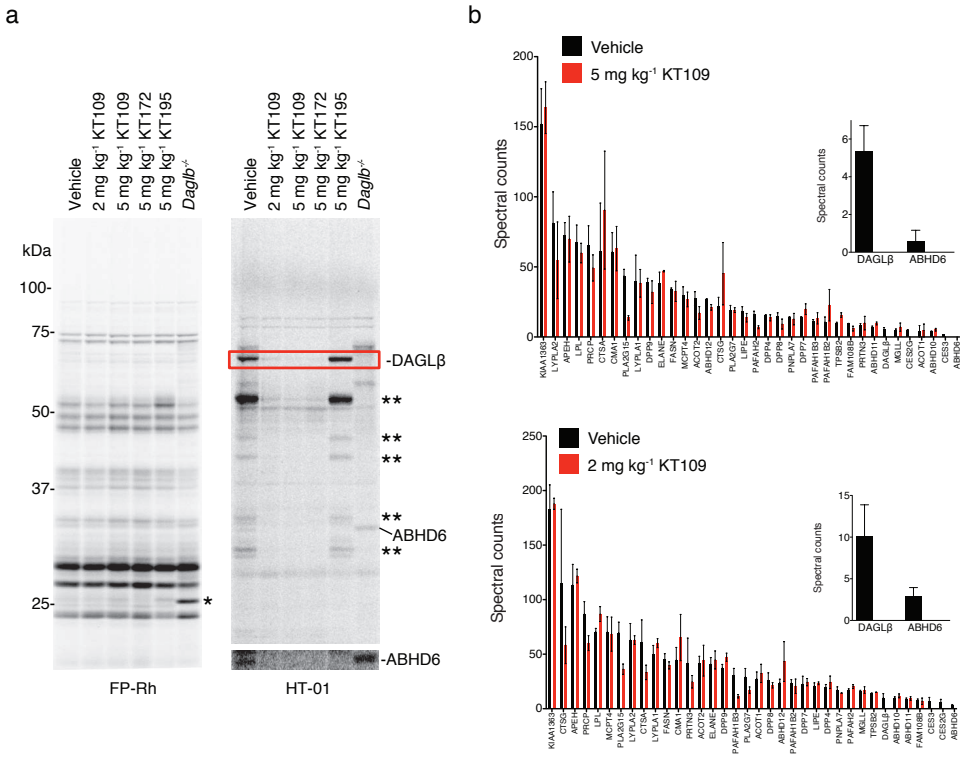

Supplementary Figure 17. Activity and selectivity of DAGLβ inhibitors in peritoneal macrophages from inhibitor-treated mice. (**a**) Competitive ABPP analysis of peritoneal macrophages from mice treated with KT109 (2 and 5 mg kg^{-1}), KT172 (5 mg kg^{-1}), or KT195 (5 mg kg^{-1}, i.p. 4 h) using both FP-Rh (1 μM, left panel) and HT-01 (1 μM, right panel). Macrophage proteomes from *Daglb*$^{-/-}$ mice are shown as a control. Single asterisk marks a 25 kDa serine hydrolase activity that is selectively observed in the 129/SvEv mouse strain in which the *Daglb*$^{-/-}$ mice were generated (this serine hydrolase activity was also detected in *Daglb*$^{+/+}$ mice; data no shown). Double asterisks designate proteolytic fragments of the DAGLβ protein that are sometimes generated and observed during sample processing. Note that these HT-01-labeled bands are not detected in *Daglb*$^{-/-}$ mice, supporting that they represent fragments of DAGLβ. For HT-01-labeled proteomes, a darker exposure of the ABPP gel is provided at the bottom of the panel to show the region that contains ABHD6 signals. (**b**) ABPP-MudPIT analysis of serine hydrolase activities from peritoneal macrophages treated with KT109 (5 and 2 mg kg^{-1}, i.p. 4 h). Treatment with KT109 completely inactivates DAGLβ (and ABHD6) at both doses tested (highlighted in inset bar graph), while not affecting most of the other 30+ serine hydrolase activities expressed in mouse macrophages. Data are presented as means ± s.e.m.; *n* = 5 mice per group.

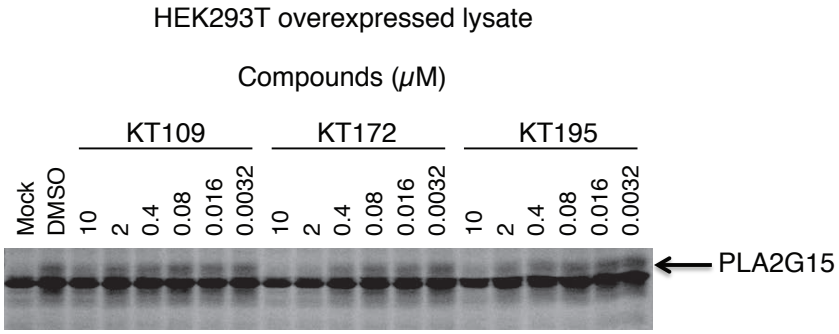

Supplementary Figure 18. Activity of DAGLβ inhibitors against recombinant PLA2G15. Competitive ABPP analysis of PLA2G15-transfected HEK293T proteome incubated with varying concentrations of KT109, KT172, or KT195 for 30 min at 37 ºC and then labeled with FP-Rh (1 μM, 30 min, 37 ºC) and separated by SDS-PAGE. PLA2G15 activity was detected by in-gel fluorescence scanning as an ~47 kDa protein not observed in mock-transfected cells. Inhibition of PLA2G15 by compounds was detected as a reduction in FP-Rh-labeling, resulting in calculated IC_{50} values of 10, 1, and 2 μM for KT109, KT172, or KT195, respectively.

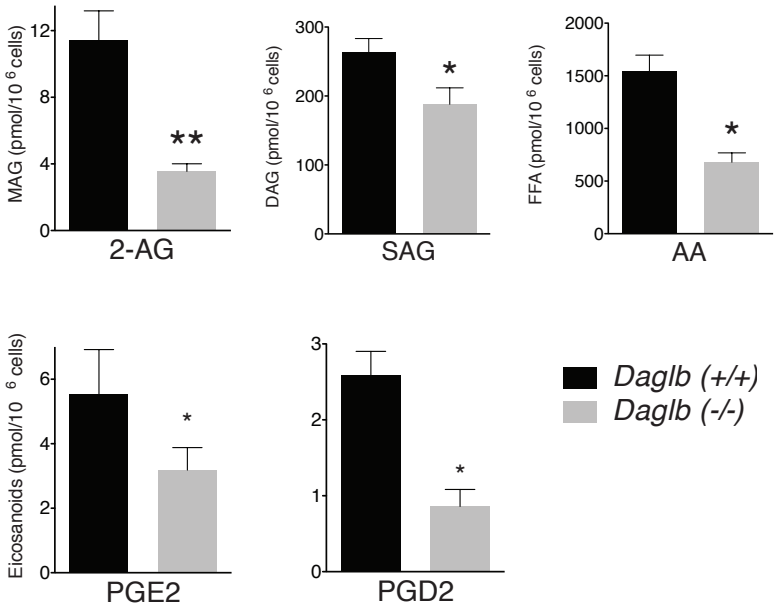

Supplementary Figure 19. Metabolomic analysis of macrophages from *Daglb*$^{-/-}$ mice. Peritoneal macrophages from *Daglb*$^{-/-}$ mice showed significantly decreased levels of 2-AG, SAG, AA, PGE_2, PGD_2 compared with macrophages from *Daglb*$^{+/+}$ mice. See **Supplementary Methods** for more detail on the metabolomics experiments. Data are presented as means $\pm$ s.e.m.; n = 3-6 mice per group. *P < 0.05; **P < 0.01 for *Daglb*$^{-/-}$ versus *Daglb*$^{+/+}$ mice.

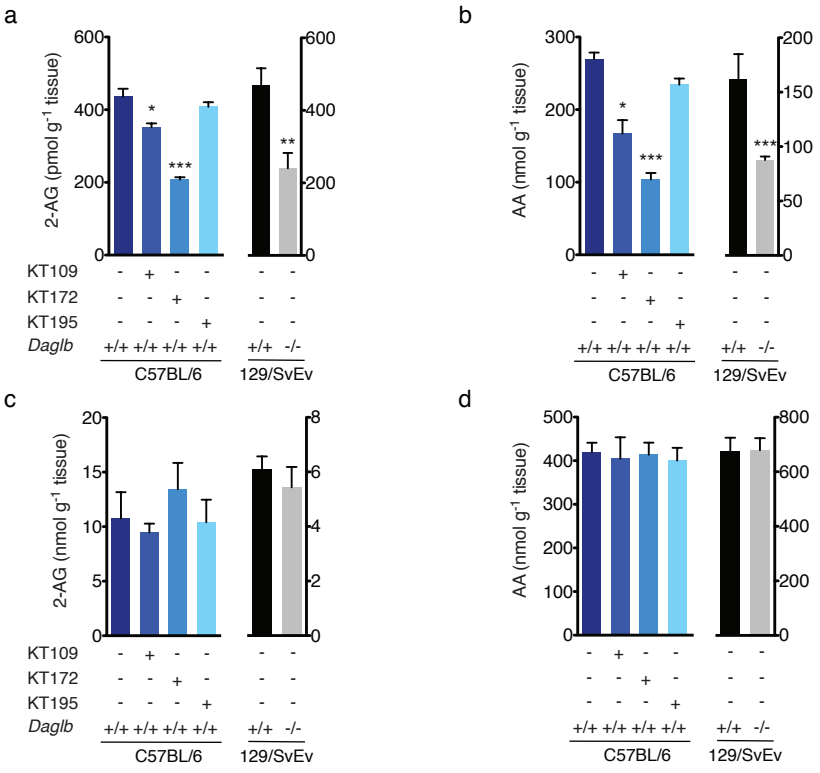

Supplementary Figure 20. Metabolomic analysis of liver and brain from KT109, KT172, and KT195-treated mice. (a-d) Levels of 2-AG (**a**) and AA (**b**) are decreased in liver tissue of mice (C57Bl/6) treated with KT109 or KT172, but not KT195 (20 mg kg^{-1}, i.p. 4 h), compared with vehicle-treated mice. Levels of 2-AG and AA are also significantly decreased in liver tissue of *Daglb*$^{-/-}$ mice compared to *Daglb*$^{+/+}$ mice (129/SvEv). In contrast, brain levels of 2-AG (**c**) and AA (**d**) are not significantly different between inhibitor- and vehicle-treated mice or between *Daglb*$^{-/-}$ and *Daglb*$^{+/+}$ mice. Data are presented as means ± s.e.m.; n = 3-5 mice per group. *$p < 0.05$; **$p < 0.01$; ***$p < 0.001$ for all inhibitor-treated groups or *Daglb*$^{-/-}$ versus vehicle-treated or *Dagl*$^{+/+}$ mice.

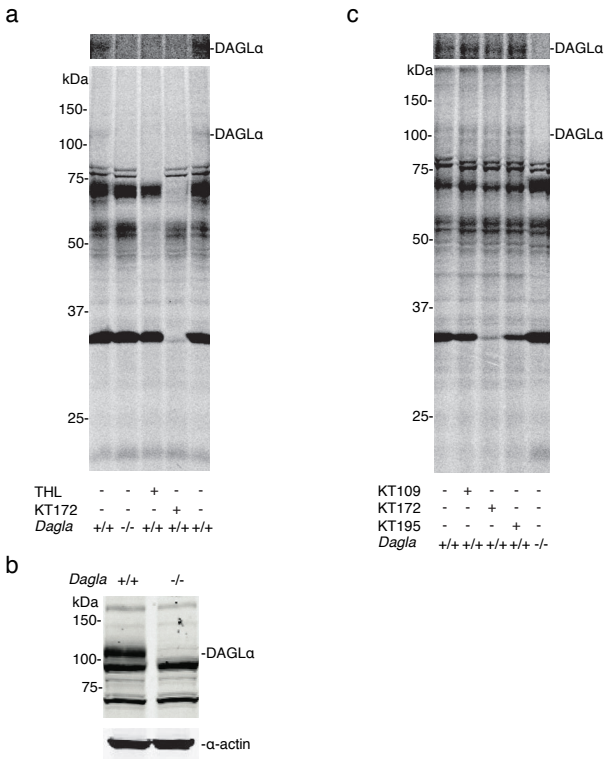

Supplementary Figure 21. The HT-01 activity probe can detect DAGLα activity in mouse brain proteomes and confirms that brain DAGLα is not inhibited by KT109 or KT172 *in vivo*. (**a**) Profiling mouse brain proteomes from *Dagla*$^{+/+}$ and *Dagla*$^{-/-}$ mice using the DAGL-directed activity probe HT-01 (1 μM). Pretreatment of mouse brain proteomes from *Dagla*$^{+/+}$ mice with THL (10 μM) or KT172 (2 μM) blocked HT-01-labeling of a ~120 kDa protein that was confirmed as DAGLα by its absence in brain tissue from *Dagla*$^{-/-}$ mice, as determined by both HT-01 labeling (**a**) and western blotting (anti-DAGLα, 1 μg/mL) (**b**). (**c**) DAGL inhibitors lack activity against DAGLα *in vivo* as judged by HT-01 labeling of mouse brain proteomes from KT109-, KT172-, or KT195-treated mice (20 mg kg^{-1}, i.p. 4 h).

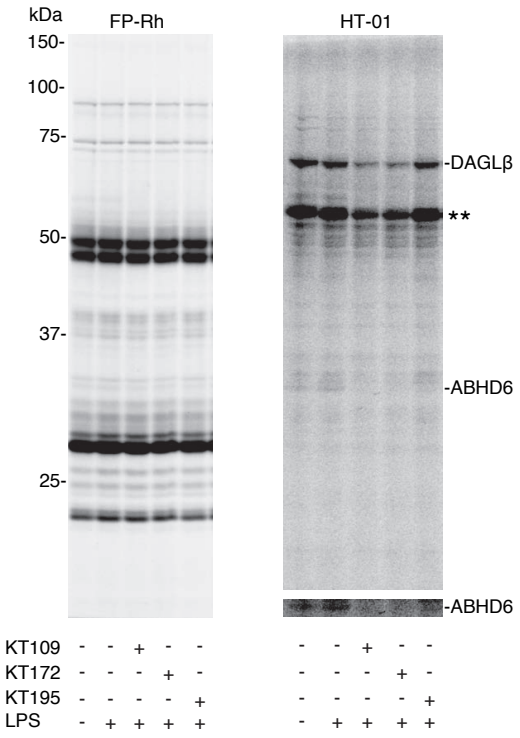

Supplementary Figure 22. Competitive ABPP of thioglycollate-elicited macrophages plated and stimulated with LPS in the presence of DAGLβ inhibitors. Competitive ABPP analysis of thioglycollate-elicited peritoneal macrophages from C57Bl/6 mice harvested as described in the **Methods** section and allowed to adhere for 4 h at 37 °C and 5% CO_2. Adhered macrophages were then washed 2X with sterile PBS and treated with KT109 (50 nM), KT172 (25 nM), or KT195 (25 nM) for 4 h, washed again with PBS, followed by stimulation with LPS (5 μg/mL) for 90 min in serum-free media. Macrophage proteomes were then labeled with either FP-Rh (1 μM) or HT-01 (1 μM) and enzyme activities detected by in-gel fluorescence scanning. KT109 or KT172 treatment results in >80% reductions in DAGLβ activity with no observable activity against any other gel-detectable serine hydrolases except ABHD6, which was also blocked by the KT195 control probe. Double asterisks designate proteolytic fragments of the DAGLβ protein that are described in **Supplementary Fig. 17**.

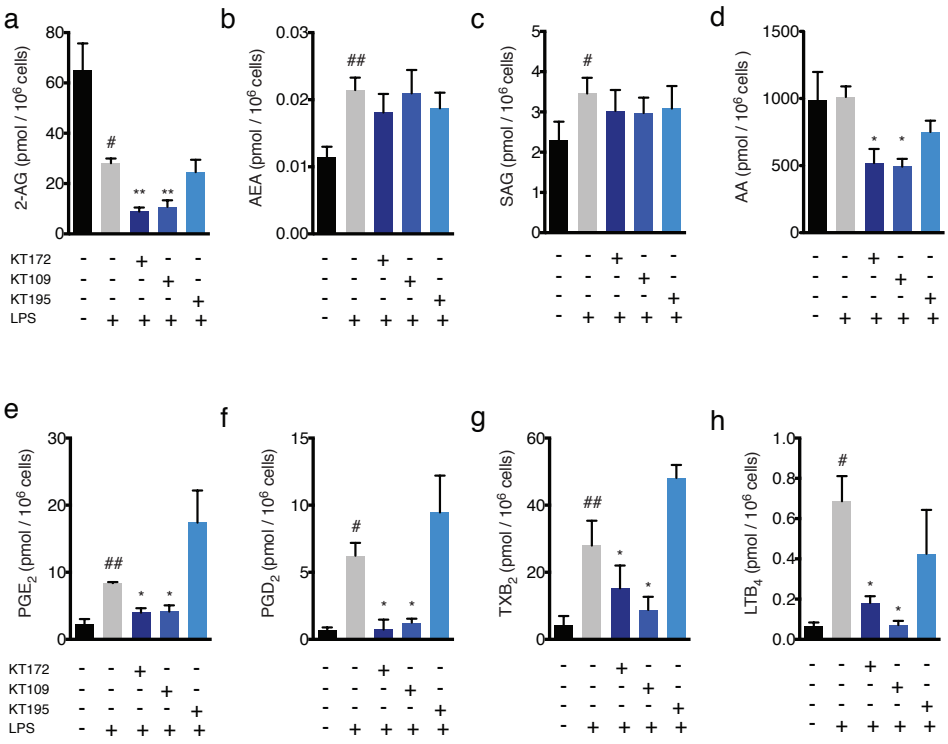

Supplementary Figure 23. Metabolomic analysis of C57Bl/6 macrophages plated and treated with compounds in the presence of LPS. Thioglycollate-elicited peritoneal macrophages from C57Bl/6 mice were harvested, plated, and treated with DAGL inhibitors as described in **Supplementary Fig. 22**, and subjected to metabolomic analysis as described in the **Methods** section. LPS stimulation significantly reduces cellular levels of 2-AG (**a**) and increases AEA (**b**), SAG (**c**), PGE2, PGD2, TXB2, and LTB4 (**e**-**h**). Pretreatment with KT109 (50 nM, 4 h) or KT172 (25 nM, 4 h), but not KT195 (25 nM, 4 h), caused significant reductions in LPS-stimulated levels of all metabolites except AEA and SAG compared with DMSO-treated macrophages. Data are presented as means ± s.e.m.; *n* = 3-5 mice per group. #$p < 0.05$; ##$p < 0.01$ for DMSO-treated groups treated with or without LPS. *$p < 0.05$; **$p < 0.01$ for all inhibitor-treated groups versus DMSO-treated macrophages in the presence of LPS.

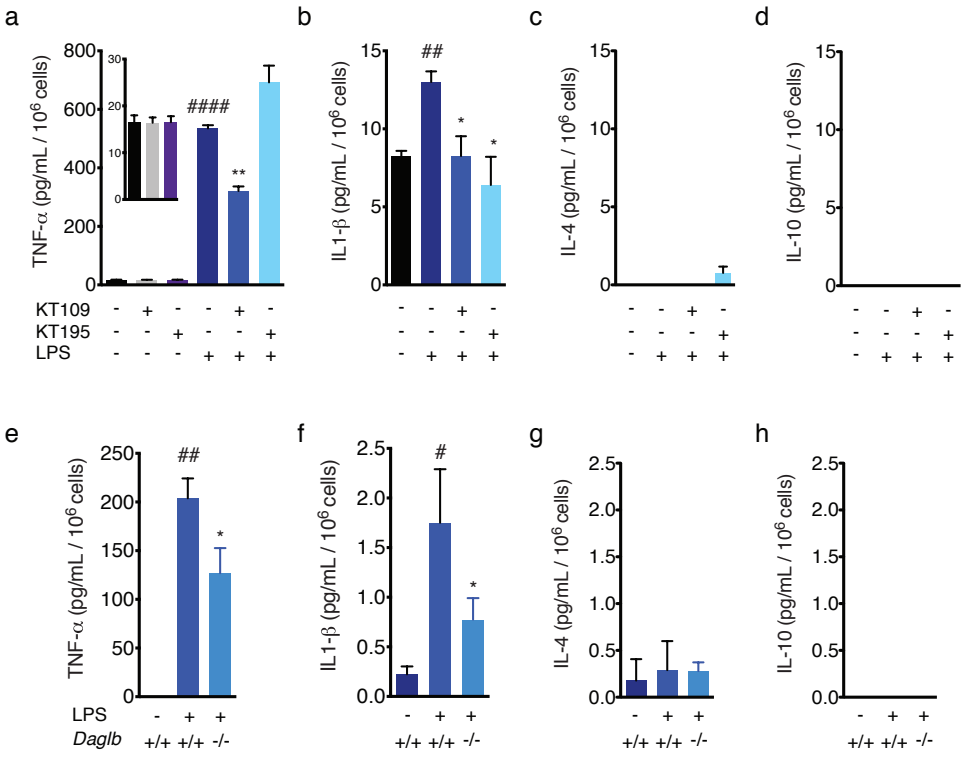

Supplementary Figure 24. Cytokine analysis of plated mouse macrophages. Thioglycollate-elicited peritoneal macrophages from C57Bl/6 (**a**-**d**) or *Daglb*$^{-/-}$ (**e**-**h**) mice were harvested and plated as described in **Supplementary Fig. 22**. C57Bl/6 macrophages were pretreated with KT109 or KT195 for 4 h as described above and all macrophages were subsequently stimulated with LPS (5 μg/mL) for 90 min in serum-free media and LPS-stimulated cytokine levels were measured as described in the **Methods** section using Single-Analyte ELISAarray kits (Qiagen) per the manufacturer's instructions. Treatment of macrophages with KT109 or KT195 did not change the baseline levels of TNF-α (**a**, inset graph). Treatment with LPS causes significant increases in secreted levels of TNF-α (**a** and **e**) and IL1-β (**b** and **f**), but not IL-4 or IL-10 (**c**, **d**, **g**, **h**) from macrophages. KT109, but not KT195 caused a significant reduction in TNF-α levels (**a**), while both inhibitors reduced LPS-stmulated levels of IL1-β (**b**). Significant reductions in LPS-stimulated TNF-α (**e**) and IL1-β (**f**) were also observed in macrophages from *Daglb*$^{-/-}$ mice compared with *Daglb*$^{+/+}$ mice. Data are presented as means ± s.e.m.; n = 3-5 mice per group. #$p < 0.05$; ##$p < 0.01$; ####$p < 0.0001$ for DMSO-treated or *Daglb*$^{+/+}$ groups treated with or without LPS. *$p < 0.05$; **$p < 0.01$ for all inhibitor-treated or *Daglb*$^{-/-}$ groups versus DMSO-treated or *Daglb*$^{+/+}$ groups in the presence of LPS.

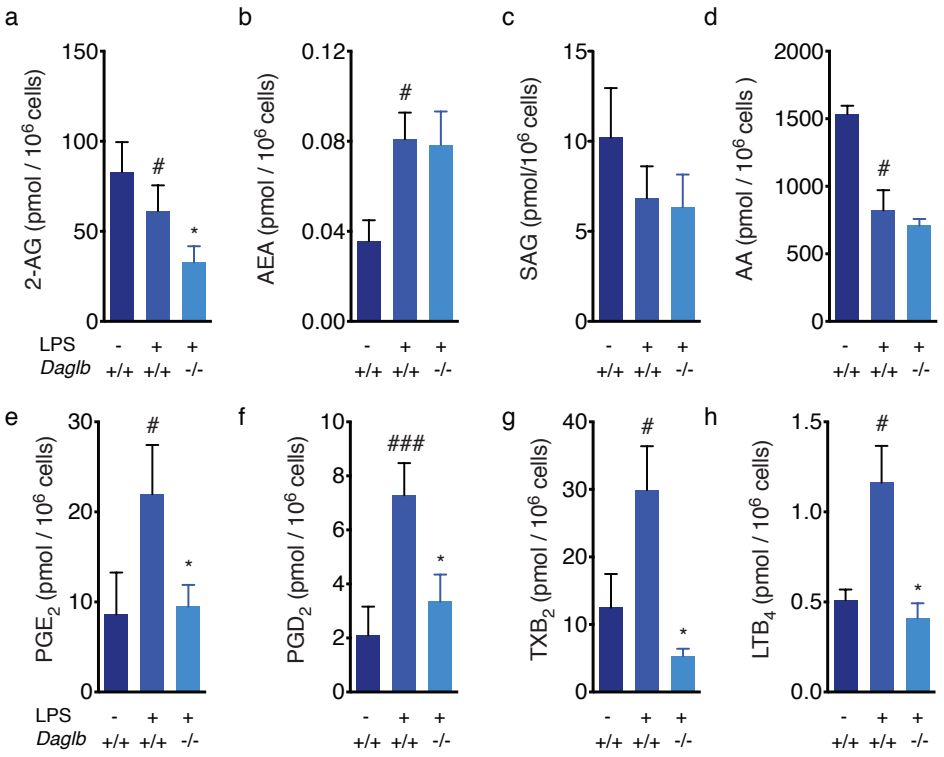

Supplementary Figure 25. Metabolomic analysis of macrophages from *Daglb*$^{-/-}$ mice plated and treated with LPS. Thioglycollate-elicited peritoneal macrophages from *Daglb*$^{+/+}$ and *Daglb*$^{-/-}$ mice were harvested, plated, and stimulated with LPS as described in **Supplementary Fig. 22**. LPS stimulation of *Daglb*$^{+/+}$ macrophages significantly reduced cellular levels of 2-AG (**a**) and AA (**d**) and increased AEA (**b**), PGE2 (**e**), PGD2 (**f**), TXB2 (**g**), and LTB4 (**h**). *Daglb*$^{-/-}$ macrophages showed significant reductions in LPS-stimulated levels of 2-AG (**a**), PGE2 (**e**), PGD2 (**f**), TXB2 (**g**), and LTB4 (**h**). Data are presented as means ± s.e.m.; *n* = 3-5 mice per group. #*p* < 0.05; ##*p* < 0.01 for *Daglb*$^{+/+}$ groups treated with or without LPS. **p* < 0.05; ***p* < 0.01 for *Daglb*$^{-/-}$ versus *Daglb*$^{+/+}$ macrophages in the presence of LPS.

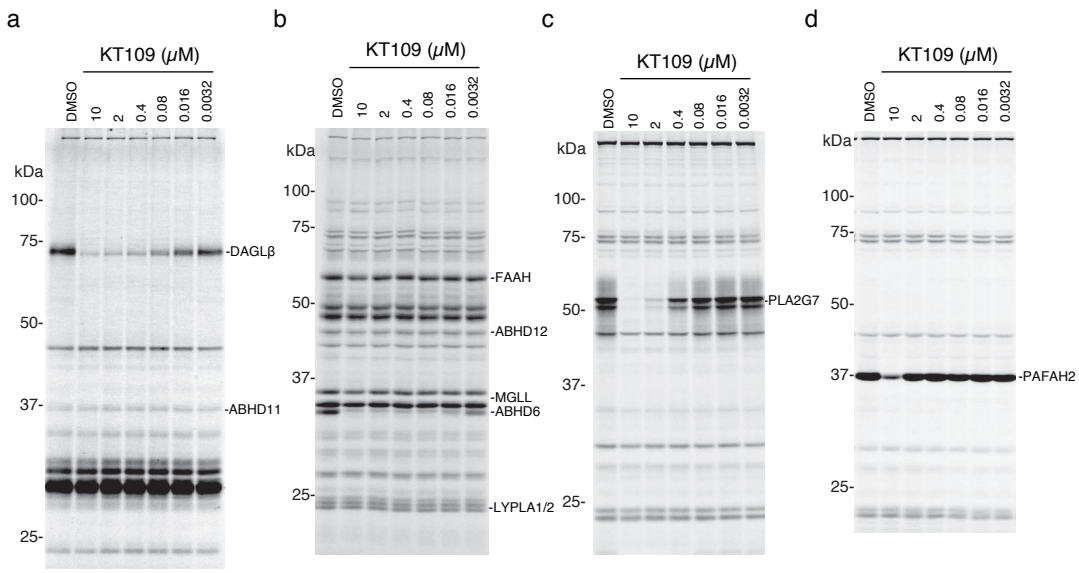

Supplementary Figure 26. Full gel images for KT109 in **Figure 1b.**

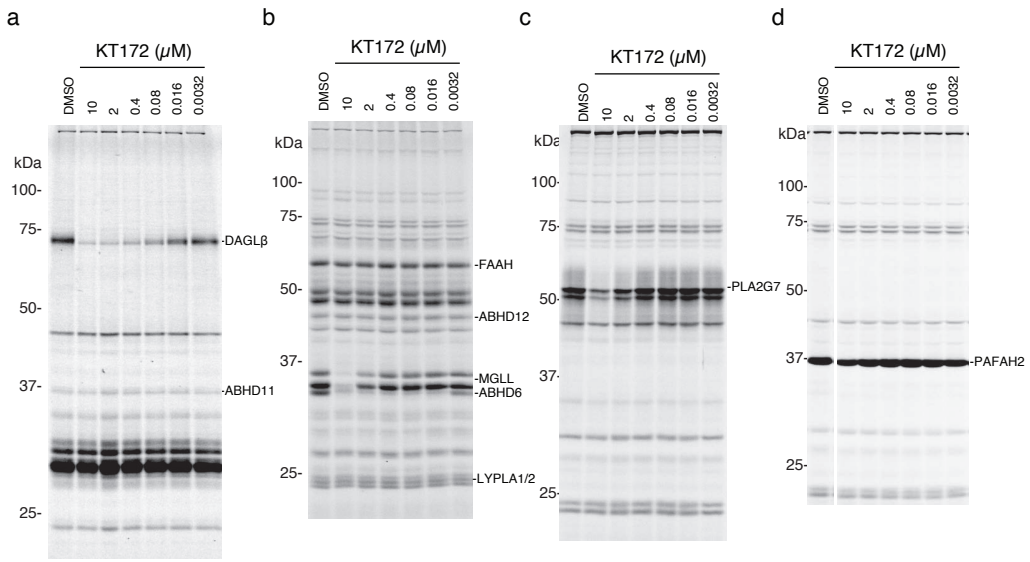

Supplementary Figure 27. Full gel images for KT172 in **Figure 1b**.

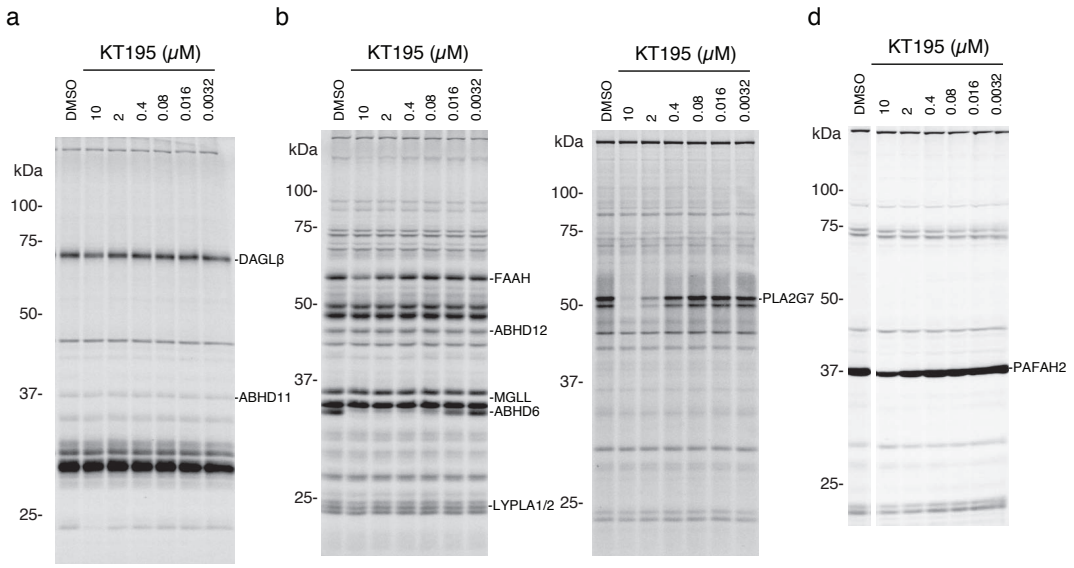

Supplementary Figure 28. Full gel images for KT195 in **Figure 1d** (DAGLβ signals) and **Supplementary Figure 7** (DAGLβ, FAAH, MGLL, ABHD12, ABHD6, ABHD11, LYPLA1/2 signals).

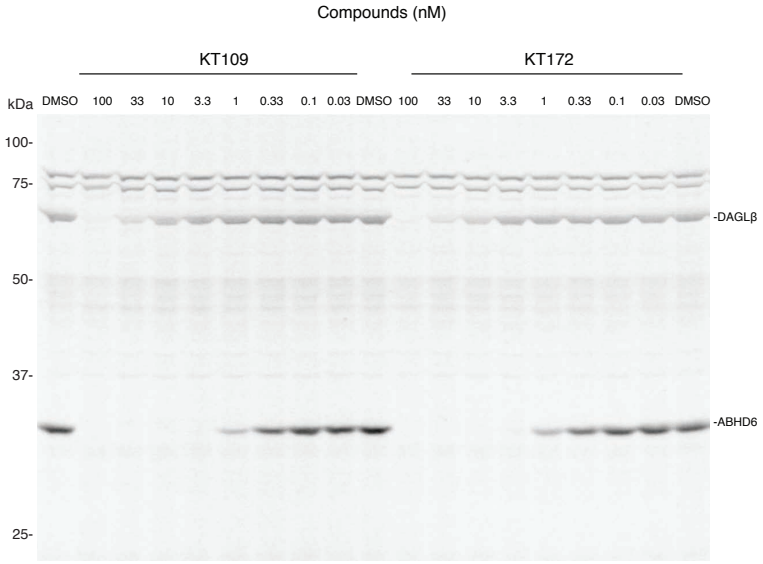

Supplementary Figure 29. Full gel images for KT109 and KT172 in **Figure 3a**.

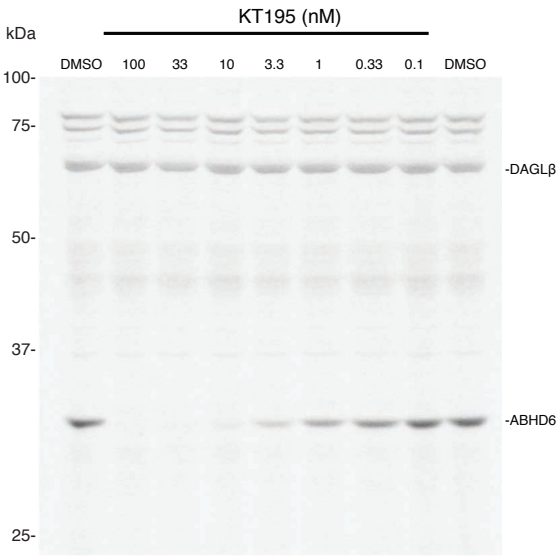

Supplementary Figure 30. Full gel images for KT195 in **Figure 3b**.

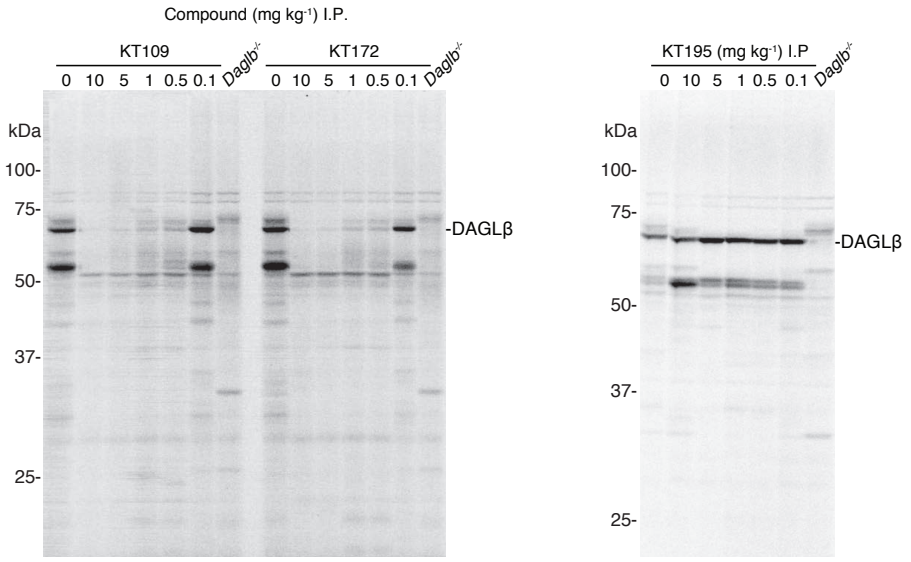

Supplementary Figure 31. Full gel images for KT109, KT172, and KT195 in **Figure 4b**.

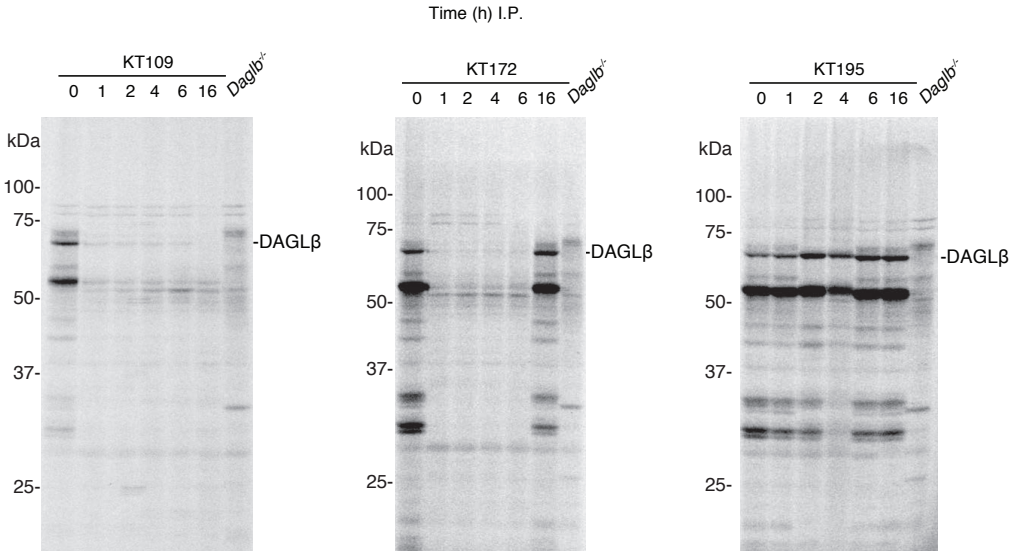

Supplementary Figure 32. Full gel images for KT109, KT172, and KT195 in **Figure 4c**.

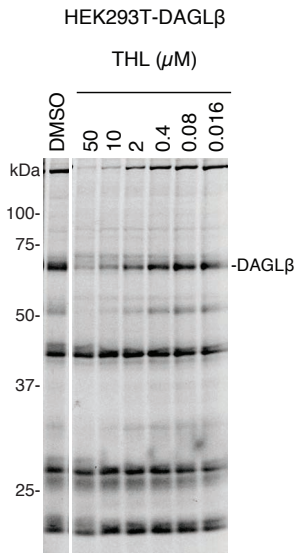

Supplementary Figure 33. Full gel image for **Supplementary Figure 1c**.

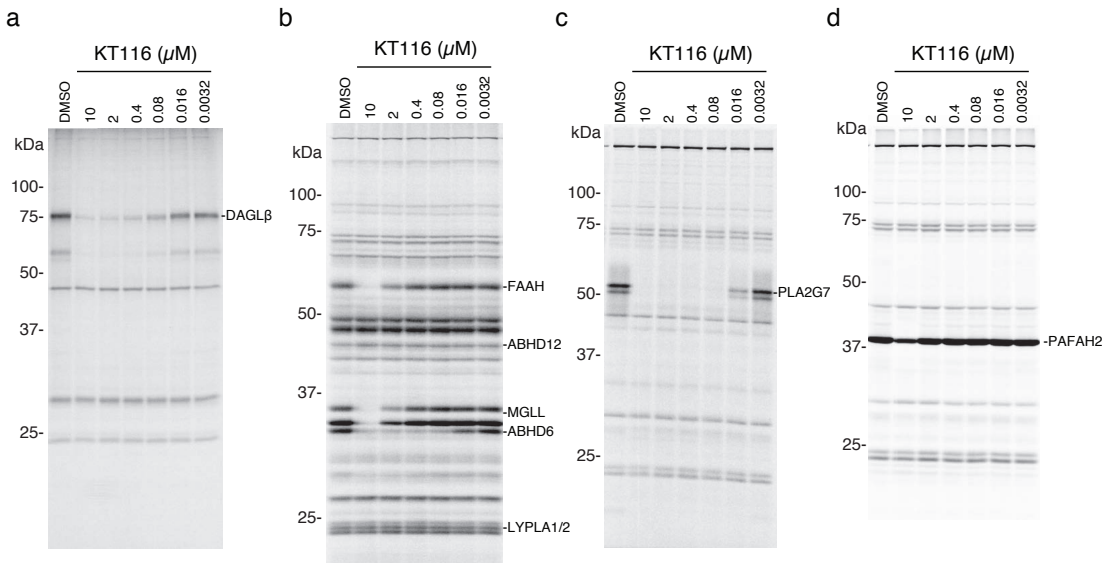

Supplementary Figure 34. Full gel images for **Supplementary Figure 3d**.

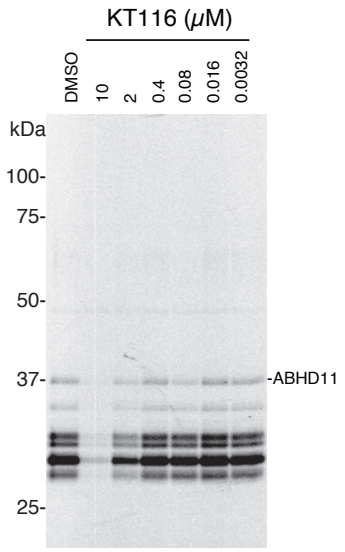

Supplementary Figure 35. Full gel images for **Supplementary Figure 3d** (ABHD11 signals).

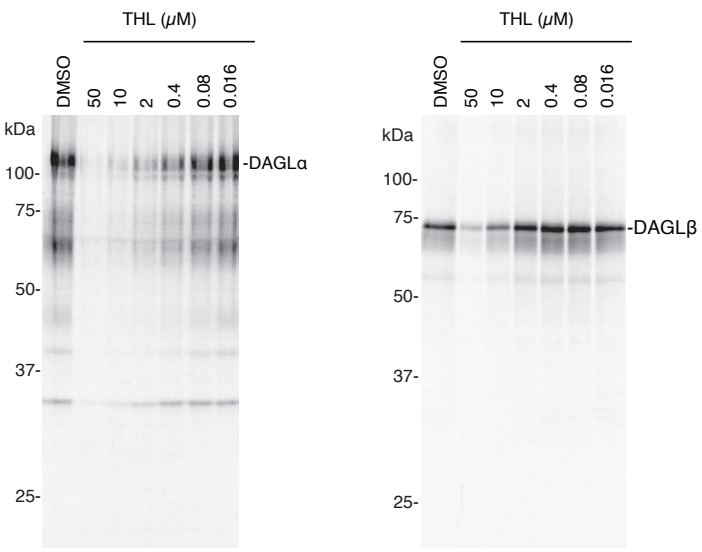

Supplementary Figure 36. Full gel image for **Supplementary Figure 5b**.

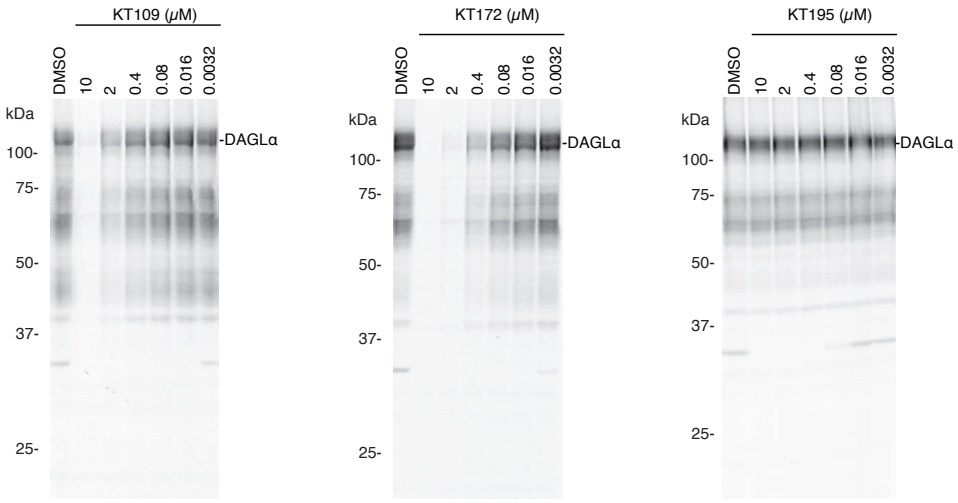

Supplementary Figure 37. Full gel image for **Supplementary Figure 5c**.

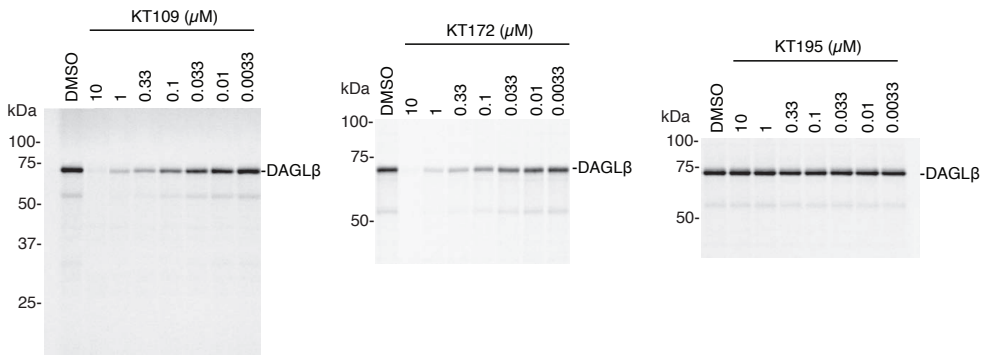

Supplementary Figure 38. Full gel image for **Supplementary Figure 5d**.

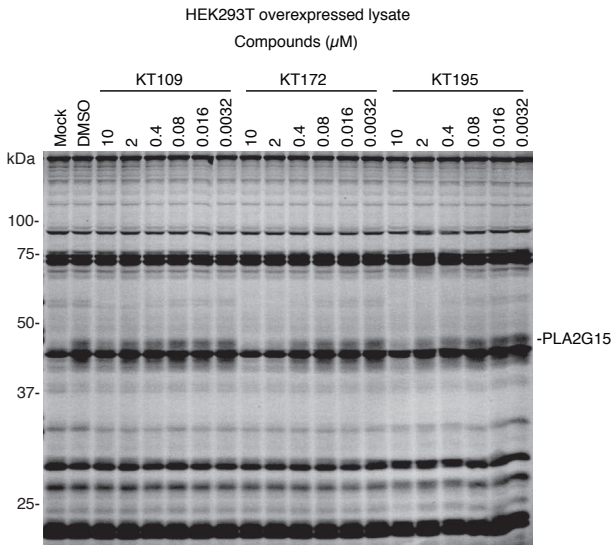

Supplementary Figure 39. Full gel image for **Supplementary Figure 18**.

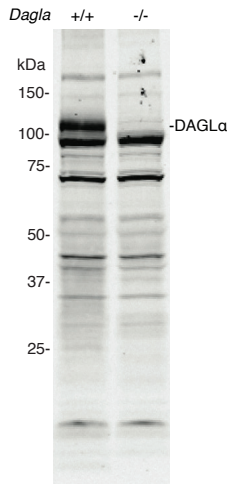

Supplementary Figure 40. Full gel image for **Supplementary Figure 21b**.